THE ASTROPHYSICAL JOURNAL, 243: 460–484, 1981 January 15

ULTRAVIOLET ABSORPTION BY INTERSTELLAR GAS AT LARGE DISTANCES FROM THE GALACTIC PLANE

BLAIR D. SAVAGE[1] AND KLAAS S. DE BOER[1]
Washburn Observatory, University of Wisconsin-Madison
Received 1980 April 28; accepted 1980 June 25

ABSTRACT

We have analyzed 18 high dispersion *IUE* spectra of six stars in the Large Magellanic Cloud, three stars in the Small Magellanic Cloud, and two foreground stars. Fourteen spectra cover the wavelengths 1150–2000 Å, and four cover 1900–3200 Å. The velocity resolution is $\sim$25 km s^{-1}. All the Magellanic Cloud star spectra exhibit exceedingly strong interstellar absorption lines due to a wide range of ionization stages at galactic velocities and at velocities associated with the LMC or SMC. In this paper the analysis is restricted to the Milky Way absorption features. Toward the LMC stars, the strong interstellar lines have a positive velocity extension to $v_{LSR} \approx 150$ km s^{-1}, which exceeds by $\sim$100 km s^{-1} the extension recorded toward the SMC stars. The most straightforward interpretation of these velocity extensions is obtained by assuming that gas at large distances away from the plane of the galaxy participates in the rotation of the galaxy as found in the galactic disk. This then indicates that we have detected absorption by gas as far as perhaps 10–15 kpc below the plane of the galaxy. Toward many of the LMC stars the low ion stage lines exhibit a component structure with strong features near 60 and 130 km s^{-1}. The presence of O I absorption at these velocities implies that a portion of the gas is neutral even though it is not detected in existing 21 cm emission data. A curve-of-growth analysis provides some information on the composition of the low-ion high-velocity gas. Solar abundances are consistent with the uncertain abundance estimates, although there is the possibility that the N/O ratio is less than solar. The high ionization lines of Si IV and C IV are strong toward all the Magellanic Cloud stars, whereas N V is not detected. These data provide definitive proof that highly ionized species exist in the general interstellar medium of our Galaxy away from local stellar environments. The weakness of the high ion lines toward the foreground galactic stars implies that the strong absorption toward the extragalactic stars is primarily produced by gas beyond $r \approx 0.9$ kpc. For this halo gas we obtain toward the LMC log N(C IV) $\approx$ 14.0, log N (Si IV) $\approx$ 13.5, and log N(N V) $<$ 13.5. Toward the SMC the N V limit is the same but the C IV and Si IV column densities are at least a factor of 2 larger. If the high ion gas is produced by equilibrium "coronal ionization," the implied temperatures are in the range $0.7-1.4 \times 10^5$ K. The high ion line profiles contain less component structure than the low ion profiles, suggesting a smoother high ion gas distribution. While the low ion gas might represent condensed material in a galactic fountain model, it is not obvious where within this model the high ion gas fits since the fountain, if it exists, is presumably driven by gas with much higher temperatures. If the high ion gas is primarily formed in "cloud coronae," one might expect to find a better correspondence between the low and high ion line profiles than is observed. Perhaps the high ion gas represents a type of "transition region" between gas in the plane of the Galaxy and a hotter exterior zone that can not be studied with *IUE* data. Assuming solar abundances, the amount of halo gas detected represents $\sim$2% of that found in the galactic disk.

Subject headings: galaxies: Milky way — galaxies: structure — interstellar: abundances — interstellar: matter — ultraviolet: spectra

[1]Guest observers with the *International Ultraviolet Explorer* satellite, which is sponsored and operated by the National Aeronautics and Space Administration, by the Science Research Council of the United Kingdom and by the European Space Agency.

I. INTRODUCTION

Until very recently, ultraviolet interstellar absorption line studies have been limited to relatively bright stars with distances ranging up to about 3 kpc from the Sun. However, the *International Ultraviolet Explorer* (*IUE*) launched in 1978 January (Boggess *et al.* 1978*a*) has provided an important new tool for interstellar research. With *IUE* it is possible to obtain high-resolution ultraviolet spectra ($\lambda/\Delta\lambda \sim 1.2 \times 10^4$) of hot, lightly reddened stars with V magnitudes as faint as +13. With this capability, the brightest stars in the Large and Small Magellanic Clouds (LMC and SMC) have become accessible for ultraviolet interstellar line research. The 55–65 kpc path to the Magellanic Clouds samples interstellar material in the disk and halo of the Milky Way and in the halos and disks of the Magellanic Clouds. The radial velocities of the Magellanic Clouds (140 km s^{-1} for the SMC and 245 km s^{-1} for the LMC) are adequate to separate the galactic and the extragalactic interstellar absorption lines. In a previous paper (Savage and de Boer 1979, hereafter Paper I) we presented *IUE* interstellar data for two stars in the LMC. In those data evidence was found for the existence of a gaseous galactic corona similar to the theoretical predictions of Spitzer (1956). In two subsequent papers (de Boer, Koornneef, and Savage 1979, hereafter Paper II; de Boer and Savage 1980, hereafter Paper III), the Magellanic Cloud part of the interstellar absorption was discussed. In Paper III it was concluded that the Magellanic Clouds are probably also surrounded by gaseous coronae.

In this paper we present the full data for the galactic interstellar absorption seen toward nine Magellanic Cloud stars. Six stars are located in the LMC and three in the SMC. These data generally confirm the conclusions presented in Paper I and provide new information about the properties of the interstellar gas far from the plane of the Milky Way.

Section II describes the observations and methods of data reduction. In § III the general aspects of the detected interstellar absorption features are summarized. Detailed comments are contained in § IV. The spectra of two galactic foreground stars in the direction of the LMC and SMC are briefly described in § V. The evidence in the data that we are detecting gas at large z distances is summarized in § VI. In the remaining sections we in turn discuss: the velocity structure of the absorption and its relation to galactic rotation (§ VII); the absorption features of the low ions (§ VIII); and the absorption features of highly ionized species (§ IX). In the last section (§ X) we comment on the relation between these new observations and current theories of gas in the galactic halo.

II. OBSERVATIONS AND REDUCTIONS

During different observing runs with *IUE* the high dispersion ultraviolet spectra listed in Table 1 were obtained. The *IUE* image numbers preceded by a 3 denote spectra obtained with the short wavelength camera which covers the wavelength range 1150–2000 Å with a velocity resolution of 25 km s^{-1}, while image numbers preceded by a 2 refer to the long wavelength spectra which extend from 1900 to 3200 Å with a velocity resolution of 30 to 20 km s^{-1} (see Boggess *et al.* 1978*a*, *b* for detailed information about the *IUE* observatory characteristics). Six of the observed stars are in the LMC , three are in the SMC, and two are foreground Milky Way stars.

All spectra except image 3-2766 were obtained through the large entrance aperture. The integration times in hours are indicated in parentheses after the image number. For the Magellanic Cloud stars these times were generally 5 hours for the short wavelength camera and 3 hours for the long wavelength camera. For the repeat exposures of HD 36402 and HD 5980, different positions of the star in the large aperture were used to permit an assessment of the fixed pattern noise in the spectra. All spectra were processed with the standard Goddard Space Flight Center processing routines (see Boggess *et al.* 1978*b* and the *IUE* newsletters) and plotted in a convenient format with our Space Astronomy Laboratory Modcomp II computer. Because of the long exposure times, the Magellanic Cloud star spectra have an enhanced background and a large number of cosmic ray spots. The photographic representation of the images (photowrites) are valuable in identifying bad data points. The background correction applied to the gross signal was taken to be a 30 point running average of the interorder background (done twice) excluding reseau dips and radiation spots. At the short wavelength end ($\lambda < 1300$ Å), where the echelle orders crowd together, this correction was obviously an overcorrection. We therefore applied an additional zero point intensity correction which typically amounted to 10% at 1280 Å and 25% at 1200 Å and was inferred from the highly saturated interstellar lines in this wavelength region.

The Magellanic Cloud stars were selected for their ultraviolet brightness, where some preference was given to stars with W-R characteristics in order to benefit from the higher fluxes in the emission part of the stellar P Cygni profiles for studying interstellar C IV, Si IV and N V. The sources for the various stellar parameters listed in Table 1 are given as footnotes to the table. The stellar radial velocities are given with reference to the local standard of rest.

In Figure 1 we illustrate sample spectra for the echelle orders containing the Si IV 1393.76 Å line and the C IV doublet at 1550.77 and 1548.20 Å. The LMC star HD 36402 is illustrated in the upper spectra and the SMC star HD 5980 is illustrated in the lower spectra. The echelle blaze function, which causes the observed falloff in intensity at long and short wavelengths, has not been corrected for in these plots.

TABLE 1

GALACTIC AND MAGELLANIC CLOUD STARS OBSERVED

LOCATION	HD	Sk[h]	Sp[a]	V[a]	B-V[a]	E(B-V)[a,b]	N(H I)[g] (10^{20} cm^{-2})	ℓ	b	V(LSR) (km s^{-1})	IMAGE NUMBER (EXP. TIME HRS, QUALITY, ITF)
LMC	HD 36402	104-67	WC5+OB	11.50	...	...	5.3	277.8	-33.0	318[c]	3-4911(5.0 Bi) 3-5768(5.0 Bk) 2-5004(3.0 Bk)
"	HD 268605	5-67	09.7Ib	11.34	-.12	.17	4.4	278.9	-36.3	293[f,d]	3-6540(5.0 Ck) 2-5613(2.3 Ck)
"	...	18-67	06-7+WN5	11.95	-.21	.09	...	278.2	-36.0	272[d]	3-4293(5.0 Cj)
"	HD 38268	243-69	OB?+WN5	9.42	+.14	.44	5.5	279.4	-31.7	245:[e]	3-2766(7.0 Dj)
"	HD 38282	246-69	WN6-A(B)	11.13	-.12	.08	5.5	279.4	-31.7	245:[e]	3-2798(5.4 Cj) 3-4258(5.0 Cj) 3-4951(5.0 Cj) 2-3766(3.0 Bk)
"	HD 269357	104-69	06Ib(f):	12.10	-.21	.11	...	279.9	-33.4	251[d]	3-4314(4.8 Dj)
SMC	...	108	06.5+WN3	12.41	-.29	.01	3.4	301.6	-45.0	129:[f]	3-4926(5.0 Bj)
"	...	80	07Iaf+	12.36	-.21	.11	3.6	302.1	-45.0	...	3-6564(5.0 Dk)
"	HD 5980	78	OB?+WN3	11.86	-.26	.04	3.6	302.1	-44.9	...	3-4277(5.0 Bj) 3-4345(3.0 Cj) 3-4958(5.0 Bi) 2-5583(3.0 Bk)
d≈900	HD 33599	...	B5	8.9	...	.09[m]	...	271.3	-35.9	...	3-6570(1.0 Aj)
d≈900	HD 10747	...	B3	8.3	...	.06[m]	...	298.9	-41.1	...	3-4297(0.8 Aj)

a For the Magellanic Cloud stars these data are mostly from Walborn (1977).

b The total (galactic + extragalactic) color excess is listed.

c From the IUE spectrum (paper III).

d Ardeberg et al. (1972).

e See Paper II.

f Feast, Thackeray, and Wesselink (1960).

g These galactic 21 cm H I column densities are from Koornneef and McGee (1981).

h Sanduleak numbers, see Sanduleak (1968, 1970).

i Processed with inferior and correct ITF.

j Processed with inferior ITF.

k Processed with correct ITF.

m Inferred from N(H I) and used in estimating the distances in column 1.

A,B,C,D Code of decreasing spectrum quality.

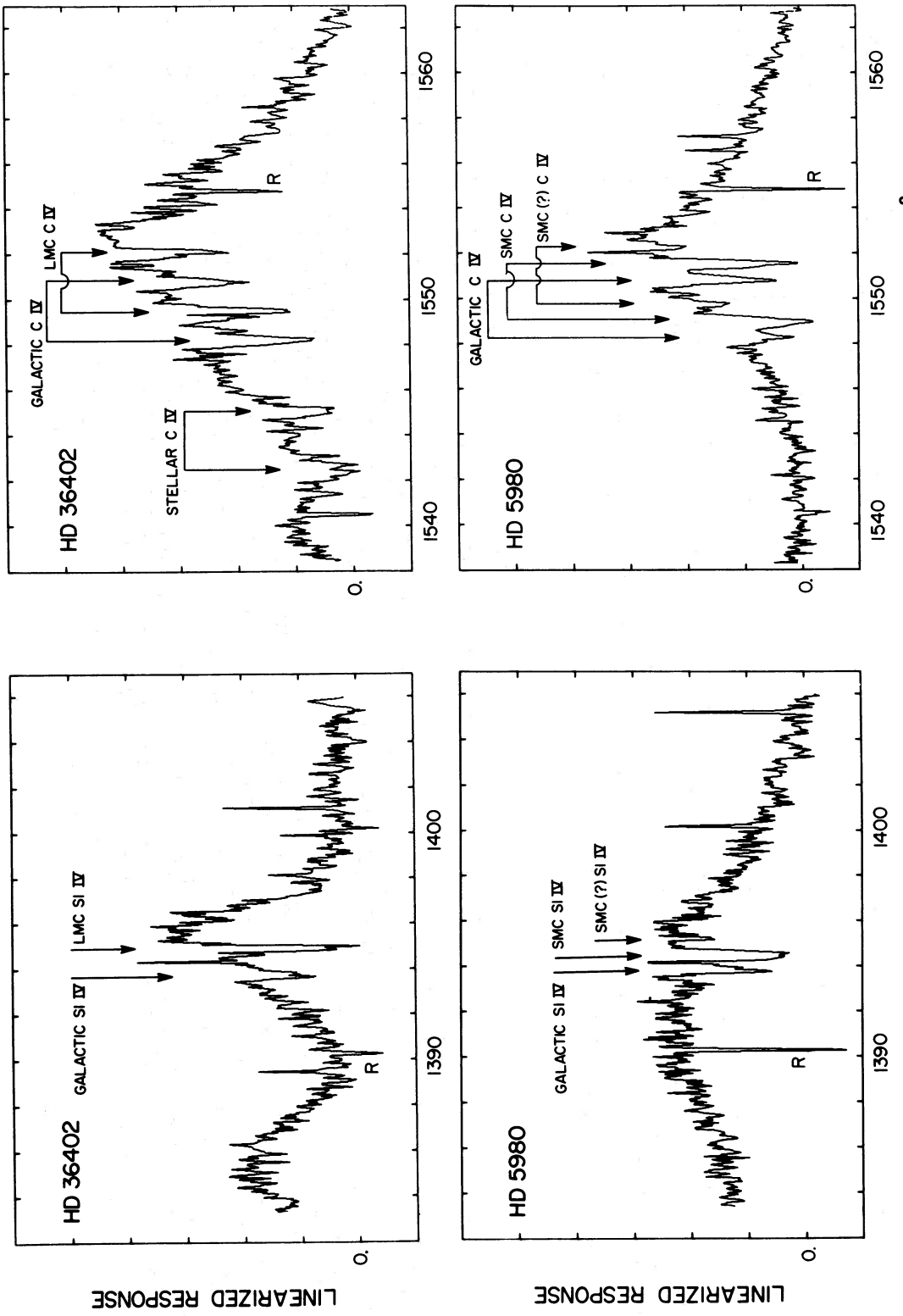

FIG. 1.—For HD 36402 in the LMC and HD 5980 in the SMC we show the complete echelle orders containing the lines of Si IV λ1393.76 and C IV λ1548.20 and λ1550.77. The data are from images 3-5768 for HD 36402 and 3-4277 for HD 5980. The echelle blaze function has not been removed and causes the signal falloff at long and short wavelengths. The stellar continua show the atmospheric P Cygni type profiles of these high ion lines. In addition, the well defined lines represent absorption due to galactic and extragalactic interstellar Si IV and C IV in the same transitions. Near the reference wavelength the interstellar absorption is due to high ion gas at galactic velocities; the strong component to the red pertains to absorption by gas in each Magellanic Cloud. Toward HD 36402 the galactic component is clearly asymmetric; toward HD 5980 an additional absorption component is seen near +300 km s^{-1}. *R* denotes a detector reseau. The features that look like emission lines in these spectra are produced by cosmic rays. These defects can be easily recognized on the photowrites.

Superposed on the stellar Si IV and C IV P Cygni profile are the interstellar Si IV and C IV lines. The galactic and extragalactic absorption components are clearly separated for both stars, although for HD 5980 the red wing of the galactic interstellar absorption blends with the SMC absorption line. For HD 5980 there is a third very high velocity component of unknown origin (see Paper III).

In order to interrelate interstellar spectral features due to different elements and ions, we have transformed the basic spectra similar to those shown in Figure 1 into intensity versus velocity plots. Samples of these plots are illustrated in Figure 2 for many of the important lines in the wavelength regions covered by the *IUE* short and long wavelength cameras. Other examples can be found in Papers I, II, and III. The transformation was to LSR velocities with the conversion: $v_{\rm LSR} - v_{\rm HELIO} = -16$ km s^{-1} for the LMC and -11 km s^{-1} for the SMC. Since various positions in the large entrance aperture were employed, it was necessary to use observed lines in the spectra to establish the zero point in the velocity plots. For the short wavelength spectra the zero point was set by making the average velocity of the three lines in the S II triplet near 1255 Å agree with the average velocity of the H I 21 cm emission profiles obtained by Koornneef and McGee (1981). For the long wavelength spectra the velocities of the middle-ultraviolet Fe II lines were forced to agree with that of the 1608.46 Å Fe II line in the short wavelength spectra. The plotted velocities for both cameras should have a 1 σ accuracy of about 5 km s^{-1}.

Many of the spectra listed in Table 1 were processed at the Goddard Space Flight Center during the interval 1978 May 22–1979 July 7. It has recently become known that the short wavelength camera linearization file (ITF file) utilized during this period contained one error. The error occurred at the 20% intensity level and will cause a distortion of line profiles. In several cases (images 3-4911 and 3-4958) we have obtained spectra reprocessed with the correct ITF in order to evaluate the importance of the problem for long exposure spectra with high background. The i,j, k code following the image number in Table 1 indicates what ITF file was used to process each image. In Paper III we illustrated for image 3-4911 that, while continuum levels were larger in the reprocessed spectrum, the line profiles were only slightly affected. Other examples of this are given in Figure 2*f* for HD 5980 (image 3-4958) and HD 36402 (image 3-4911). For these two stars the correctly processed data are plotted with dots while the incorrectly processed data are plotted with a solid line. The intensities in the reprocessed spectrum were scaled in producing the plot to match the old and new continuum levels. On examining the old and new reduction we again conclude that *line profiles* for spectra with *high backgrounds* are only very slightly influenced by the ITF error. For low background spectra, D. Leckrone (private communication) has found that the ITF error can affect the depth of lines by up to ~20% of the continuum level. Since all our Magellanic Cloud data have high background levels, we conclude that the ITF problem does not significantly influence our data. The exception is the data for the two foreground galactic stars. In the present paper, however, we make only minor use of these spectra (see § V). Finally, we note that our highest quality spectra (HD 36402 and HD 5980) were processed with the correct ITF.

The spectra we have obtained vary in quality. In Table 1 we have indicated following each image number a crude A, B, C, D code of decreasing data quality. The highest quality spectra are the short-exposure galactic spectra. The long-exposure Magellanic Cloud spectra are inferior to the best *IUE* spectra of bright stars. In the following discussions, more emphasis will be placed on the Magellanic Cloud star data of highest quality.

Figure 2*f* illustrates for the C II line the reproducibility of different *IUE* long-exposure spectra of the same star. Many other examples are provided by comparing Figure 2 with Figure 1 of Paper III. In general, different spectra of the same star compare favorably. However, in these long-exposure spectra there are occasional glitches caused by nonuniformities in the background, cosmic ray spots, bad pixels, fixed pattern noise, etc. Therefore, two spectra are required in establishing the reality of weak lines ($W_\lambda \lesssim 50$ mÅ) or in judging the shapes of spectral lines.

After careful inspection of the regions of the spectra near the Si IV, C IV, and N V lines, we find that there are instrumental blemishes, which show up more clearly in the spectra obtained at later times. With the normal object position in the large aperture, both lines of the Si IV λ1396 doublet have persistent high pixels near 0 km s^{-1} while in addition the Si IV λ1402.77 line probably has a persistent high spot near 280 km s^{-1}. These bad pixels are often not obvious in a spectrum because they are frequently in or near an interstellar absorption feature. However, their existence is clear from the intercomparison of spectra of the same star obtained with different positions in the large aperture. The C IV lines both suffer from "black" pixels, near 240 km s^{-1}, while in N V there usually is a low point near 220 km s^{-1}. The bad pixels are not necessarily located exactly in the echelle spectrum, but with the large extraction slit they unavoidably are read as a stellar signal. We do not know whether the strengths of these blemishes depend on the exposure time or on the level of the particle background during the exposure. Their occurrence in Si IV near 0 km s^{-1} may indicate photometric fatigue due to frequent observations of strong emission lines. Also, we can describe them rather accurately only in the Si IV, C IV, and N V lines because of the intrinsic interest in those absorptions. Lines from other species may show similar but still undiscovered problems.

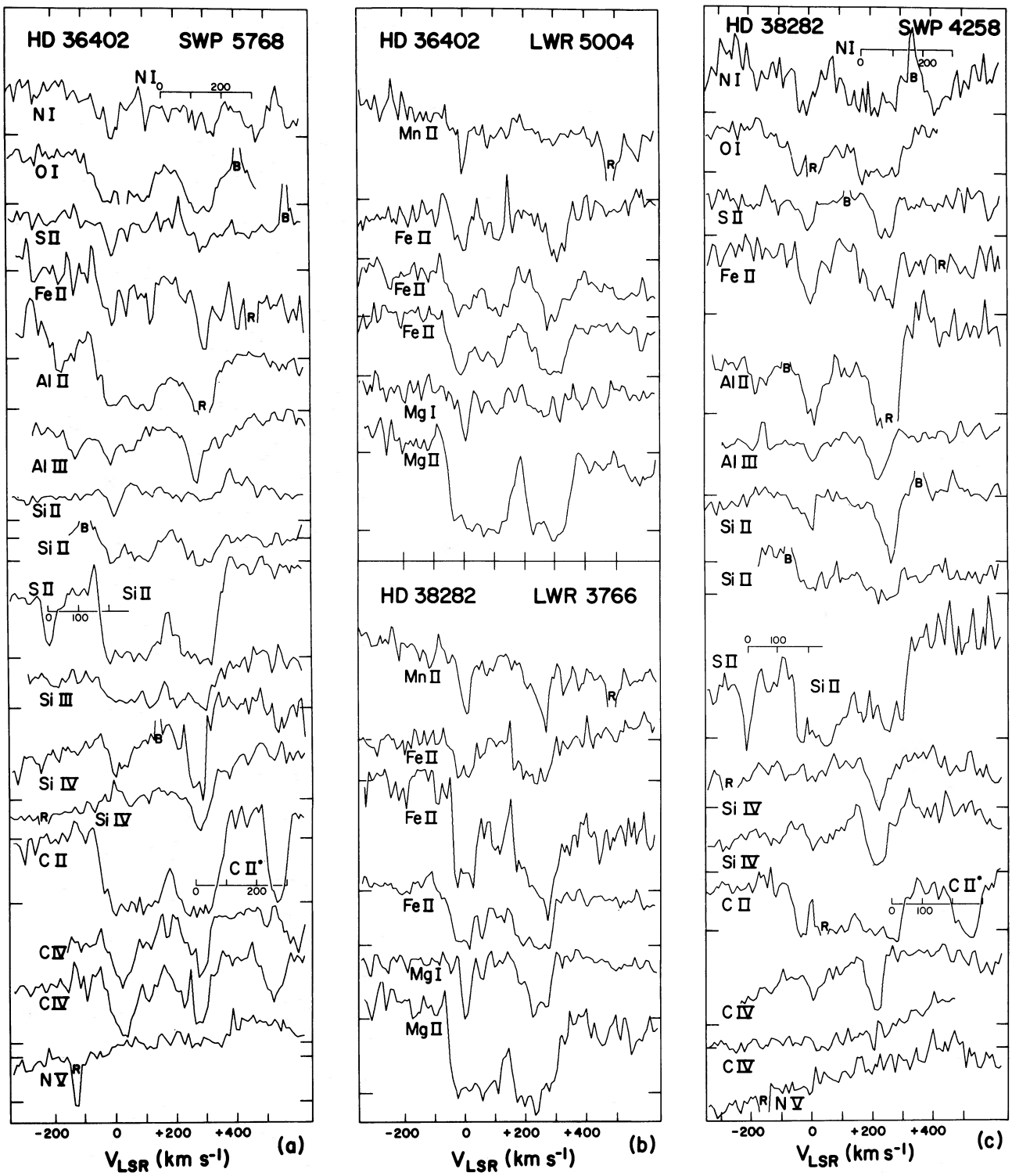

FIG. 2.—Velocity plots for interstellar absorption lines detected in Magellanic Cloud star spectra. The profiles are shown in velocity units (km s^{-1} LSR) versus net linearized response with tick marks at the appropriate zero levels. The spectra have not been rectified. Figs. 2*a*, 2*c*, 2*d*, and 2*e* show the following interstellar lines from the short wavelength images: N I λ1199.55 and λ1200.22 (partly blended), O I λ1302.17, S II λ1253.81, Fe II λ1608.46, Al II λ1670.79 from two orders, Al III λ1854.72, Si II λ1808.00, Si II λ1304.37, Si II λ1260.42 (see Table 2 note 1) with to the left S II λ1259.52, Si III λ1206.51 (not shown for HD 38282), Si IV λ1402.77, Si IV λ1393.76, C II λ1334.53 and to the right partly blended C II* λ1335.7, C IV λ1550.77, C IV λ1548.20, and N V λ1242.80. Fig. 2*b* shows the following interstellar lines from

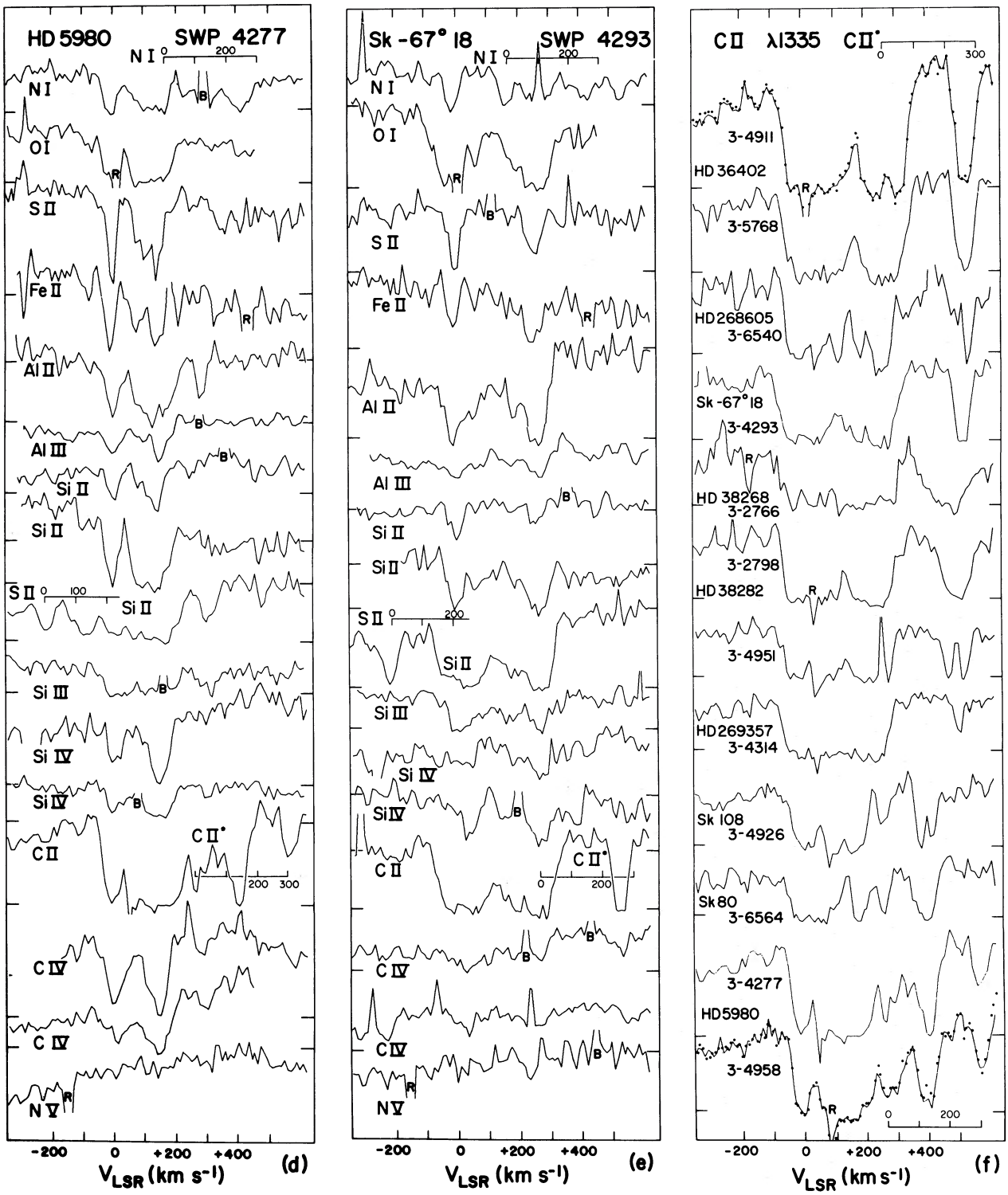

the long wavelength images: Mn II λ2576.11, Fe II λ2585.88, Fe II λ2343.49, Fe II λ2599.40, Mg I λ2852.13 and Mg II λ2795.53. In the plots, B represents a "bad pixel" and R a reseau (see text). Fig. 2*f* shows the C II λ1334.53 line for most of the available images, arranged according to the galactic longitude of the star (as in Table 1), to show change with longitude, repeatability from image to image, and the extreme width of the C II line. Other examples of these plots can be found in Papers I, II, and III. The image repeatability can best be inferred by comparing data in this figure with Figure 1 in Paper III. With dots we show the same profile processed with the correct ITF (see § II). Similar information is shown for C IV and Si IV in Paper III.

TABLE 2

VELOCITIES AND EQUIVALENT WIDTHS OF GALACTIC INTERSTELLAR LINES TOWARD MAGELLANIC CLOUD STARS

Species		Notes	f	HD 36402			HD 268605			Sk −67 18			HD 38268		
				v_-	v_+	W_λ	v_-	v_+	W_λ	v_-	v_+	W_λ	v_-	v_+	W_λ
C I	1656.93	d	0.136	−5	+25	50	n	n	n	−25	+25	150s	−20	+20	50
	1277.24	d,w	0.156	−10	+25	80	−27	+28	40:	−30	+10	70:	n	n	n
C II	1334.53	a,h	0.118	−52	+175	970b	−47	+98	660	−70	+120	780b	−65	≡+140b	≥700b
C II*	1335.7	d,h	0.118	h	h	h	h	h	h	h	h	h	h	h	h
C IV	1550.77	g	0.097	−15	+55	190	−7:	+53:	250:	+5	+45	140	f	f	f
	1548.20	e	0.194	−15	+75	330	n	n	n	−10:	+70:	450::	f	f	f
N I	1200.22	i	0.088	−22	n	n	−22	+23	150:	−25	+20	190	n	n	n
	1199.55	i	0.133	−32	+23:	210:g	−7	+28	140:	−35	+15	190	n	n	n
N V	1242.80		0.0757	...	...	<30	...	...	<50	...	...	<40	n	n	n
	1238.82	e	0.152	n	n	n	...	...	<50	e	e	e	n	n	n
O I	1302.17	a,u	0.0486	−50	+28	320	−47	+53	420y	−70	+40	460u	−55	+60	460
Mg I	2852.13	a,w	1.77	−14	+21	230	−32	+43	260	q	q	q	q	q	q
	2025.82	j,w	0.110	−15	+18	40	−17	+23	70	...	...	<50	...	...	...
Mg II	2802.70	c	0.295	−51	+148	1800	−42	+45	850	q	q	q	q	q	q
	2795.53		0.592	−49	+146	1950	−42	+153	1900b	q	q	q	q	q	q
Al II	1670.79	a,c	1.88	−40	+45	480	−27	+33	410y	−35	+30	350	−35:	+75:	500:
Al III	1862.79	k	0.268	−32	+8	100::	n	n	n	−30	+5	60:	−30	+25	100:
	1854.72	k	0.539	−17	+20	120::	−32	+13	140:	−30	+25	160:	−25	+55	150:
Si II	1808.00		0.0037	−7	+23	85	−12	+18	110	−20	+20	120	−40	+20	200
	1526.72	a	0.0764	−35	+35:	320	a	n	f	a	+15	310	−70	+55	650
	1304.37	w	0.147	−30	+28	260	−37	+58	500	−30	+30	230	−40	+45:	440
	1260.42	l	0.959	−42	+160	820	−52	+155	900:	−50	+110:	670b	−60	≡+140	≥700b
	1193.28	c,w	0.500	−33	+145	750	n	n	n	−70	+85	600	n	n	n
Si II*	1264.8	d	0.959	...	...	<50	...	...	<40	...	...	n	...	...	<50
Si III	1206.51	e	1.66	−45	+83	450	−37	+23	220:f	−25	+100	480	n	n	n
Si IV	1402.77		0.262	g	g	140:	g	+53	160:g	g	g	g	f	f	f
	1393.76	e	0.528	−22	+110	240	−27	+83	350	+15	+65	180	f	f	f
S II	1259.52	v	0.0159	−22	+20	120:	−22	+23	170:	−27	+20	180:	n	n	n
	1253.81		0.0107	−17	+13	100	−22	+23	130	−20	+15	170	−15	+10	100
	1250.59	a	0.0054	−15	+20	90	−22	+18	140	−15	+15	120	f	f	f
Cr II	2055.59	w	0.109	−10	+20	35	...	...	<60	...	...	...	...	...	...
Mn II	2605.70		0.158	−14	+16	160	−17	+13	140	q	q	q	q	q	q
	2593.73		0.223	−19	+16	200	−17	+18	270	q	q	q	q	q	q
	2576.11		0.288	−19	+11	180	−22	+18	320	q	q	q	q	q	q
Fe II	2599.40		0.203	−44	+26	570	−52	+28	650y	q	q	q	q	q	q
	2585.88	c	0.0573	−39	+26	400	−37	+30	460	q	q	q	q	q	q
	2382.03		0.328	−34	+26	500	−22	+23	380	q	q	q	q	q	q
	2373.73		0.0395	−19	+26	300:	−12	+28	300:	q	q	q	q	q	q
	2343.49		0.108	−34	+26	500	−32	+43	400	q	q	q	q	q	q
	1608.46	w	0.035	−30	+15	180	−37	+28	250	−30	+10	120	−20	+10	250
Ni II	1741.56		0.068	−20	+15	40	−22	+23	60:	−10	+25	50	...	...	...
Zn II	2062.02		0.202	−10	+20	60	...	...	...	−30	+15	110:	−20	+20	150:
	2025.51	j	0.412	−20	+23	120	−22	+23	170	−30	+15	180	−20	+20	150

TABLE 2—*continued*

				HD 38282			HD 269357			Sk 108			Sk 80			HD 5980		
Species	λ	Notes	f	v_-	v_+	W_λ	v_-	v_+	W_λ	v_-	v_+	W_λ	v_-	v_+	W_λ	v_-	v_+	W_λ
C I	1656.93	d	0.136	-4	+28	70	-26	+9	70	...	...	...	n	n	n	n	n	n	-8	+22	35
	1277.24	d,w	0.156	-6	+35	50	-6	+24	60	...	...	...	-8	+22	40:	...	...	<40	-18	+10	30
C II	1334.53	a,h	0.118	-56	+134b	850b	-61	≡+185b	≥1100b	p	p	b,p	-33	+52b	390b	-44	≡+40	≥400b	-35	+32b	290b
C II*	1335.7	d,h	0.118	h	h	h	h	h	h	+40	+180	<50	-13	+27	110	-20	+20	140	-18b	+68	260m
C IV	1550.77	g	0.097	-15	+40:	140:t	-6	+39	140:	...	...	...	-23	+52	410s	-33	+40	230	-28	+48	330
	1548.20	e	0.194	0:	+30:	200:	-6:g	+59:g	360:g	...	...	...	-18	+47	360	-20	+40	310:	-27	+45	330b
N I	1200.22	i	0.088	i	i	i	-46	+4	200:	i	i	i	i	i	i	i	i	i	i	i	i
	1199.55	i	0.133	-50	+14	250:	-46	+14	200:g	g	g	g	-43:	+22	270:	n	n	n	-35	+18	220
N V	1242.80		0.0757	...	...	<40	...	...	<40	...	...	...	...	...	<30	...	...	<90	...	...	<30
	1238.82	e	0.152	n	n	n	...	...	<50	...	...	...	...	...	<100	n	n	n	n	n	n
O I	1302.17	a,u	0.0486	-59	+85	590	-61	+69	460	+104	+184	310	-28	+27	260	a	a	a	-30	+23	200
Mg I	2852.13	a,w	1.77	-11	+24	320	q	q	q	q	q	q	q	q	q	q	q	q	-25	+10	260
	2025.82	j,w	0.110	-23	+11	60	...	...	...	...	...	...	j	j	j	f	f	f	-7	+18	35
Mg II	2802.70	c	0.295	-51	+74	1530b	q	q	q	q	q	q	q	q	q	q	q	q	-28	+15	360
	2795.53		0.592	-51	+124	1630b	q	q	q	q	q	q	q	q	q	q	q	q	-20	+20	380
Al II	1670.79	a,c	1.88	-50	+67	600	-36	+64	490	+89	+174	500b	-18	+32	320	-20	+28b	220b	-22	+28	300
Al III	1862.79	k	0.268	-21	+14	60	-21	+24	80:	...	...	...	-23	+17	40	...	...	<40	-20	+22	60
	1854.72	k	0.539	-13	+24	90	-41	+34	130	...	...	...	-13	+17	110	n	+30	80:	-22	+22	90
Si II	1808.00		0.0037	-23	+16	140	-16	+29	130	...	...	...	-18	+29	100	-20	+18	110	-20	+22	130
	1526.72	a	0.0764	-50:	+30:	430y	a	+29	310:y	+99	+169	320b	a	a	a	a	a	a	-28	+22	230
	1304.37	w	0.147	-49	+67	420	-36	+29	250y	+94:	+184:	190:b	-43	+27	290	-20	+13	100:	-22	+22	170
	1260.42	l	0.959	-54	+137	780b	-61	≡+185	≥1040b	p	p	p	-28:	+52	270:b	-9:	+38:	240:b	-32	+38b	290b
	1193.28	c,w	0.500	-55	+33	340	-46	+49	380	+94	+184b	360b	-33	+47	320	n	n	n	-27	+23	180
Si II*	1264.8	d	0,959	...	...	<30	...	...	<50	...	...	...	...	...	<30	...	...	<50	...	...	<30
Si III	1206.51	e	1.66	-26	+38	250	-21	+64	370	+74	≡+185	>450b	-23	≡+57	≥320b	-27	+43b	260b	-22	+33	230b
Si IV	1402.77		0.262	-21	+24	90:	-16:	+49:	120:g	g	s	s	-23	n	n	-32	+36	200	-22	+22	150
	1393.76	e	0.528	-16	+35	170	+4	+44:f	150:f	s	s	s	-23	+42	270	-22	+23	180	-22	+38	190
S II	1259.52	v	0.0159	-24	+17	170	-21	+19	170:	...	...	...	-13	+22	150	-20	+16	110:	-25	+15	110
	1253.81		0.0107	-36	+12	130	-26	+19	150	...	...	...	-23	+12	110	-42:	+3	130	-18	+12	120
	1250.59	a	0.0054	-16	+22	140	-21	+14	100	...	...	...	-15	+19	90	-22	+18	100	-15	+18	100
Cr II	2055.59	w	0.109	...	...	<40	...	...	...	...	...	...	...	...	<50	...	...	<40	-38	+20	60
Mn II	2605.70		0.158	-11	+19	130	q	q	q	q	q	q	q	q	q	q	q	q	...	...	<70
	2593.73		0.223	-16	+14	190	q	q	q	q	q	q	q	q	q	q	q	q	-20	+5	110
	2576.11		0.288	-16	+24	210	q	q	q	q	q	q	q	q	q	q	q	q	-10	+20	80
Fe II	2599.40		0.203	-46	+34	670y	q	q	q	q	q	q	q	q	q	q	q	q	-30	+15	360
	2585.88	c	0.0573	-33	+34	470y	q	q	q	q	q	q	q	q	q	q	q	q	-22	+18	340
	2382.03		0.328	-36	+24	480y	q	q	q	q	q	q	q	q	q	q	q	q	-30	+10	290
	2373.73		0.0395	-52	+26	380	q	q	q	q	q	q	q	q	q	q	q	q	-30	+5	300
	2343.49		0.108	-41	+39	550y	q	q	q	q	q	q	q	q	q	q	q	q	-40	+15	460
	1608.46	w	0.035	-28	+17	240	...	...	...	-16	+14	250	+94	+144	60	-33	+17	290	-42	+8	180	-35	+15	170
Ni II	1741.56		0.068	-13	+15	70	...	...	...	-5	+45:	50	...	...	...	n	n	n	-12	+23	40:	-13	+12	30
Zn II	2062.02		0.202	-14	+14	60	...	...	...	-16	+19	90	...	...	...	-1	+17	45	-22	+13	60:	-10	+12	30
	2025.51	j	0.412	-23	+11	130	...	...	...	-21	+4	45:	...	...	...	-23	+9	100	-22	f	f	-17	+13	70

NOTES TO TABLE 2

Wavelengths are vacuum below 2000 Å, air above 2000 Å (in Paper II all λ's were vacuum). The velocities v_- and v_+ are in km s $^{-1}$ LSR, W_λ is in mA. The *f*-values are from Morton and Smith (1973), but with revisions discussed under (w) below.

:Uncertainty larger than normal (see § II).

::Uncertainty much larger than normal (see § II).

[a]Reseau near or in absorption line; for very wide lines this may not be a problem.

[b]Galactic and Magellanic Cloud components blend; therefore the measurement is uncertain. If the blending is severe, lower limits to W_λ are given based on the velocity extension seen in other absorption lines. The ≡ symbol indicates the assumed velocity.

[c]Measurements are sometimes based on two echelle orders.

[d]Unresolved blend within the same multiplet.

[e]Line is usually near the bottom of a stellar line; therefore the W_λ's are often less reliable.

[f]Cosmic ray spot contaminates the measurement.

[g]Bad pixel or instrumental artifact may contaminate the measurement.

[h]The C II and C II* lines are separated by 264 km s $^{-1}$. For LMC stars, C II at Magellanic Cloud velocities blends with Milky Way C II* with $v \lesssim 80$ km s $^{-1}$. However, we can infer the absence of high-velocity Milky Way C II* toward the LMC. Toward the SMC the Milky Way C II* is free from blending except for HD 5980 (see comment m).

[i]Close lines of N I triplet. In SMC spectra λ1199.55 is blend-free. In LMC spectra λ1200.22 is sometimes resolved. W_λ is only given for resolved lines.

[j]Mg I λ2025.82 and Zn II λ2025.51 are separated by 46 km s $^{-1}$. The reported Mg I equivalent widths may be affected by blending. The measurements are from the short wavelength spectra.

[k]In some of the spectra the continuum near the Al III lines contains structure that may be of stellar origin; the measurements are less reliable.

[l]Si II λ1260.42 blends with the usually weaker Fe II λ1260.54 and very weak C I λ1260.74 lines. For LMC spectra, S II λ1259.52 at LMC velocities also blends into Galactic Si II. In all cases, the Si II λ1260.42 W_λ reported is the total equivalent width.

[m]Blends with high-velocity C II absorption at 295 km s $^{-1}$ (see Paper III).

[n]Data very noisy, measurement omitted.

[p]Galactic component near $v = 0$ km s $^{-1}$ blends with high-velocity component; the W_λ given is for both components.

[q]No long wavelength spectra available.

[s]Line unusually strong for unknown reason.

[t]C IV λ1550.77 is absent in image 3-4951 possibly due to an instrumental blemish; this discrepant measurement was not included in the average.

[u]The weak line of P II λ1301.87 may influence the negative velocity side of the O I λ1302.17 absorption.

[v]S II λ1259.52 W_λ measurements in orders 110 and 109 often disagree by up to a factor of 2. The average result is given.

[w]Improved *f*-values are available since the compilation by Morton and Smith (1973) for C I by de Boer and Morton (1979) and for Cr II by Abbott (1978). For Si II, revisions were adopted from the paper by Morton (1978), but Shull and York (1977) commented that the *f*-values of Si II λ1304.37 and λ1190.42 more likely have to be a factor of 2 larger. We have retained the numbers from Morton (1978), but in some of our spectra that factor could be the difference between normal and deviant abundance ratios. Morton (1978) derived an experimental *f*-value for Fe II λ1608.46 from a low-resolution scan of that line present in the low sensitivity range of *Copernicus*. We give the 6 times smaller *f*-value from Kurucz and Peytreman (1975) instead, because that value gives a good fit to the curves of growth discussed in § VIII. (See note added in proof.)

[y]Cases for which an intermediate velocity component can be separated from the low and high velocity absorptions given in Table 1. The component velocities and equivalent widths are listed below. The total galactic equivalent width is found by summing the W_λ's for all three components. For strong lines the components near 60 km s $^{-1}$ usually blend with the low velocity absorption. In these cases the equivalent widths reported in Table 2 include both features. The velocity limits of the reported absorption can be used to infer what components are included in the equivalent widths reported.

Star	Species	λ	v_-	v_+	W_λ
HD 38282	Si II	1526.72	+40	+70	130
	Fe II	2599.40	+44	+74	200
	Fe II	2585.88	+60	+70	100:
	Fe II	2382.03	+44	+69	190
	Fe II	2343.49	+60	+70	70:
HD 269357	Si II	1526.72	+34	+64	130
	Si II	1304.37	+39	+69	100
HD 268605	O I	1302.17	+53	+103	180
	Al II	1670.79	+55:	+90:	100:
	Fe II	2599.40	+58	+78	80

The basic measurements of this paper are contained in Table 2 where we list, for each Magellanic Cloud star, information about the Milky Way part of the ultraviolet interstellar line spectrum. The table contains information on velocities and absorption equivalent widths for all detected lines. In making these measurements we have assumed that the Milky Way interstellar absorption is restricted to $v_{LSR} \lesssim 180$ km s^{-1} for LMC stars and for $v_{LSR} \lesssim 80$ km s^{-1} for SMC stars. On the basis of the overall galactic and extragalactic absorption pattern this separation appears reasonable (see Fig. 4 and Paper III). The v_- and v_+ velocities indicated in Table 2 refer to the LSR velocity at which the Milky Way absorption reaches 50% of the maximum absorption depth on the low (v_-) and high (v_+) velocity sides of the profile. In those cases where different absorption components are clearly resolved we have listed velocities and equivalent widths for the individual components. When only one interstellar component is listed, the absorption equivalent width reported refers to the total equivalent width of the galactic feature. In cases where more than one spectrum is available or where more than one echelle order contains a given line, the results listed are averages. The footnotes to the table contain an extensive list of comments about the difficulties associated with individual measurements.

Various Milky Way absorption lines were not detected with an equivalent width upper limit of about 50 mÅ in those spectra of quality B and C. These lines include: N V λλ1242.80 and 1238.82; O I λ1355.60; Si II* λ1264.74; C I* + C I** λλ1329.10 and 1329.58; and CO λλ1447.36 and 1419.04.

It is not easy to reliably assess the errors in the equivalent widths reported in Table 2. In the long-exposure spectra we often see spurious features having equivalent widths of about 50 mÅ, but in certain parts of the spectra a detection limit of about 20 mÅ for narrow lines is possible. For the strong lines (>200 mÅ), the uncertainties associated with the continuum placement and blending between the galactic and extragalactic features can introduce errors of perhaps 15%. The linearization of the data may introduce additional errors. Through some footnotes to Table 2 we have attempted to identify those measurements that are not particularly trustworthy. These include those measurements identified with a colon and those measurements denoted with the letter b for which severe blending occurs between the galactic and extragalactic interstellar features. The latter case is a particular problem for many of the strong lines toward SMC stars where the velocity separation between galactic and extragalactic absorption is small. When the data were particularly noisy, we have deleted the measurement entirely and entered the letter n in the appropriate column of Table 2. The short wavelength entries for HD 36402, HD 38282, and HD 5980 represent the average over two or more images and should be more reliable than entries based on only one image.

III. GALACTIC INTERSTELLAR ABSORPTION TOWARD MAGELLANIC CLOUD STARS: AN OVERVIEW

Below we summarize the general characteristics of the ultraviolet absorption at galactic velocities detected toward Magellanic Cloud stars as reported in Table 2 and illustrated in Figure 2 and in a simplified form in Figures 3 and 4. Detailed comments about individual lines of sight are given in § IV. To facilitate the discussion we divide the UV absorption lines detected into four groups: (1) the weak lines of the low ions C I, S II, Zn II, Cr II, Si II λ1808.00, Mg I, Fe II λ2373.73, Ni II, and Mn II; (2) the strong lines of the low ions C II, Si II, and Mg II; (3) the intermediate strength lines of the low ions O I, Al II, Si II, and Fe II; and (4) the lines from the higher ions Al III, Si IV, and C IV. Si III, which is sometimes seen in the wing of Lα, seems to behave more like a strong low ion. The separation outlined above characterizes in a convenient way the nature of the detected absorptions to each star, and it is the basis for the summarizing velocity bar chart illustrated in Figure 4 which shows the approximate velocity range of absorption at half strength for representative ions in the different groups for galactic and extragalactic interstellar lines. Similar plots were given in Papers II and III.

The galactic interstellar absorption toward Magellanic Cloud stars has the following general characteristics:

1. The weak low ion lines usually exhibit only detectable absorption near 0 km s^{-1}.

2. The strong low ion lines exhibit exceedingly strong absorption features. Toward LMC stars these lines extend to very large positive velocities (to ~175 km s^{-1}), while toward the SMC stars less velocity extension is recorded (to ~50 km s^{-1}).

3. Toward LMC stars the low ion lines of intermediate strength often reveal the presence of distinct components of intermediate and high positive velocities. Also, for lines with moderate saturation the absorption tends to show an asymmetric extension to positive velocities, in some cases suggesting a separate component near 60 km s^{-1}. Toward SMC stars the component structure is not obvious.

4. The high ion lines toward all stars are very strong and generally exhibit maximum absorption near $v_{LSR} \approx$ 0 km s^{-1}. For LMC stars the strong C IV and Si IV lines usually show asymmetric extensions of absorption to large positive velocities. For example, toward HD 36402, C IV and Si IV have significant absorption to $v_{LSR} \approx 140$ km s^{-1}. Toward the SMC stars the positive velocity extension is smaller, although blending with extragalactic absorption confuses the situation.

5. For LMC stars, in those cases where the high ion lines are well observed, high velocity components are sometimes detected. However, the component structure is much less pronounced in the high ion lines than in the low ion lines. For example, toward HD 36402 the component at 120 km s^{-1} clearly detected in O I, Si II, Si III, Mg I, and Fe II is seen only weakly in C IV and not detected in Si IV.

6. The N V lines, which are a diagnostic of 2×10^5 K collisionally ionized gas, are not detected at Milky Way velocities.

7. The only line detected from an excited fine structure level is the C II* λ1335.70 line. Toward SMC stars this line is strong and exhibits a 50 km s^{-1} positive velocity extension. Toward LMC stars the Milky Way line is hopelessly blended with the LMC C II λ1334.53 line for $v\lesssim70$ km s^{-1}; higher velocity C II* is not detected.

IV. GALACTIC ABSORPTION ALONG INDIVIDUAL LINES OF SIGHT

This section contains detailed comments about the interstellar absorption along all the individual lines of sight. We have attempted to identify those situations where the Milky Way absorption profiles can be separated into components. Information on data quality is also given. The stars are ordered according to increasing galactic longitude.

a) LMC stars

For *HD 36402* the *IUE* spectra available are of the highest quality we have obtained for an LMC star (see Figs. 2*a*, 2*b*, and Fig. 3). The noise in these spectra can best be inferred from Figure 1 which shows the full echelle orders for the regions of the Si IV and C IV lines. The overall absorption pattern for HD 36402 agrees with the summary comments of § III. The C II line has a very large positive velocity extension to $v_+\approx175$ km s^{-1}. The intermediate-strength low ionization lines of O I, Mg I, Si II, and Fe II clearly reveal the presence of a blend of high-velocity absorption components with maximum absorption centered near 120 km s^{-1}. Another component near 70 km s^{-1} appears in many of the profiles. In the measurements of Table 2, absorption by the 70 km s^{-1} component was included in the equivalent widths listed for the high velocity component. It is clear that higher quality data would reveal a complicated collection of components extending from low to high velocity. The high ion lines of C IV and Si IV have profiles very different from those for the low ions. Instead of having pronounced high velocity absorption components, the high ion lines have maximum absorption near 0 km s^{-1} with a relatively smooth extension of absorption to 140 km s^{-1}. The C IV λ1550.77 and 1548.20 lines do exhibit the 120 km s^{-1} component, but it is relatively weak. This component is not obvious in the well observed Si IV λ1393.76 line. Galactic N V λ1242.80 is not detected toward HD 36402. The weak features that might be attributed to N V and that appear near 100 km s^{-1} in spectrum 3-4911 and near 120 km s^{-1} in 3-5768 are of instrumental origin.

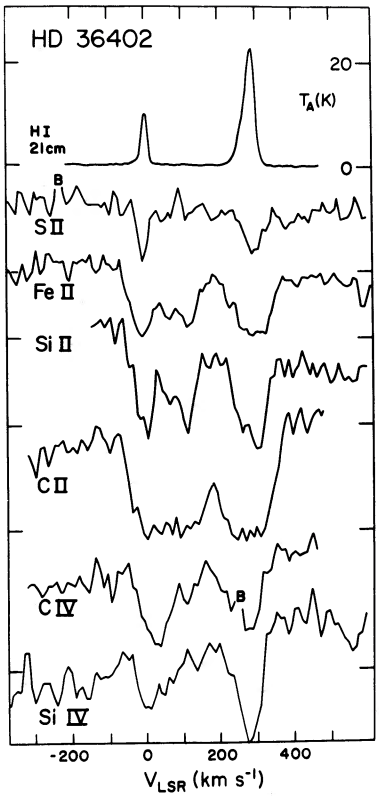

FIG. 3.—The most characteristic shapes of absorption profiles of interstellar lines are collected from the spectra available for HD 36402 in the LMC. Net linearized response not corrected for echelle blaze is plotted versus LSR velocity. The zero level of each profile is indicated with the appropriate tick mark. For a summary discussion see § III. The lines plotted include: S II λ1253.81, Fe II λ2599.40, Si II λ1304.37, C II λ1334.53, C IV λ1548.20, and Si IV λ1393.76, from the correctly processed images: 3-4911 (S II, Si II, Si IV), 3-5768 (C II, C IV), and 2-5004 (Fe II). Note the well defined high velocity components seen in Fe II and Si II, and the smoothness of the high ion absorption lines. C IV has a weak component near 120 km s^{-1} that is confirmed in the other C IV profiles. At the top we give the 21-cm H I emission profile of Koornneef and McGee (1981). No high-velocity clouds are readily apparent in their profiles except for the component associated with the LMC at ~ 280 km s^{-1}.

The short wavelength spectrum of *HD 268605* is of lower quality than the ones obtained for HD 36402. For the low ions, which have strong absorption at ~0 km s^{-1}, the lines of Mg I, O I, Si II, and Fe II show absorption extensions to positive velocities, in some cases suggesting an absorption component near 60 km

s^{-1}. There is a well defined absorption component near 130 km s^{-1}, seen in O I, S II, C II, Al II, Si II, Fe II, and Si III. At yet higher velocities there is a component at 190 km s^{-1} which we believe pertains to the LMC. The C IV and Si IV lines, which suffer from instrumental high pixels in the spectra, are strong. The C IV λ1550.77 line seems to indicate absorption near 25 km s^{-1} and also at 120 km s^{-1}. The continuum near 1242 Å is too noisy to ascertain N V absorption.

The lower quality spectrum of *Sk −67°18* shows maximum low ion absorption near 0 km s^{-1} and a positive velocity extension in the low ions suggestive of a component near 65 km s^{-1}. Here, however, there is no indication of an absorption component near 130 km s^{-1}. The LMC absorption sets in at 150 km s^{-1} in C II, and at slightly larger velocity also in O I, Si II, Al II, C II, and Si III. We cannot exclude that this absorption is due to a galactic component between 150 and 210 km s^{-1} (see the Al II line). The Si IV lines show absorption centered at +40 km s^{-1}, as does the C IV. This is at variance with the other lines of sight described. However, we may be misled by the instrumental blemishes, which may mask stronger absorption near 0 km s^{-1}. It is not clear from the line profiles if other high ion velocity components are present. Galactic N V is not detected.

HD 38268 and 38282 have been outlined in part in Paper I and in Paper II. For HD 38282 we have three short-wavelength spectra without velocity shifts, and for HD 38268 only one short-wavelength spectrum of rather low quality. Data from this latter spectrum, entered in Table 2, probably have the largest uncertainties of the whole collection. The Si IV and C IV lines, seen in the three spectra of HD 38282 which were obtained in months 8, 13, and 15 of *IUE*'s life, in particular show the decrease of the photometric quality near the nominal wavelength of these lines, as discussed in § II. Nevertheless, the high ion lines are strong and markedly asymmetric, possibly due to a component near 60 km s^{-1} LSR. This component manifests itself clearly in Mg I, O I, and the weaker Fe II and Si II lines. At 125 km s^{-1} a component is detected in Al II, Si II, and Fe II. Blades (1980), Walborn (1980), and Blades and Meaburn (1980) have observed Ca II H+K in the direction of HD 38268. Absorption components are seen near +50 and +130 km s^{-1} (LSR). These data confirm in the visual the existence of these high velocity clouds.

Toward *HD 269357* we have detected a high velocity component at 140 km s^{-1} in the low ions, notably seen in O I, Al II, Si II, Fe II, and possibly in Si III. The low ion absorption at 0 km s^{-1} shows also the extension to positive velocities, suggesting a component near 60 km s^{-1}. The C IV and Si IV lines of this spectrum are poorly defined but nevertheless collectively suggest absorption centered near 30 km s^{-1}. There may be Si IV absorption between 115 and 280 km s^{-1}, but the continuum is weak. The Si III line could indicate multiple structure. The region near N V is too noisy to ascertain any detection of that line.

b) SMC stars

The limited velocity separation between Galactic and SMC absorption makes it more difficult to analyze the Milky Way part of the absorption toward SMC stars. In preparing Table 2 we have attributed absorption with $V_{LSR} > 80$ km s^{-1} to the SMC. However, it is certainly possible that galactic absorption is occurring with these velocities. Moreover, SMC absorption at $V_{LSR} < 80$ km s^{-1} might contaminate the galactic features. The Milky Way part of the SMC star spectra definitely exhibits less positive velocity extension than for LMC stars. Since most of the galactic absorption occurs over a relatively narrow velocity range, less information is available in the SMC spectra on profile differences between high and low ions.

For *Sk 108* the high ion lines of C IV λλ1550.77 and 1548.20 and Si IV λ1393.76 are well observed and very strong. The region of the Si IV λ1402.77 line is too noisy to permit a reliable measurement of W_λ. The Si III λ1206.51 galactic and SMC lines are so strong that we see nearly total absorption between 0 and 200 km s^{-1}. C II* λ1335.70 exhibits maximum absorption near 0 km s^{-1} with an asymmetric extension to positive velocities. For N V λ1242.80 there is the possibility of a feature near 0 km s^{-1}, but we can quote only the equivalent width upper limit given in Table 2. Pronounced differences between the low and high ion line profiles are not obvious, although different ions tend to have different negative and positive velocity extents.

For *Sk 80* the short-wavelength *IUE* spectrum is noisy; many of the interstellar lines are not well enough observed to permit worthwhile equivalent width or velocity measurements. However, the galactic C IV and Si IV lines are reasonably well observed and are strong. There is no evidence for galactic N V. The galactic C II λ 1334.53 line appears anomalously wide but may be influenced by a nearby detector reseau.

The *IUE* data for *HD 5980* are the highest quality Magellanic Cloud high-dispersion data available. The data from image 3-4277 illustrated in Figure 2 can be compared to the data from image 3-4958 shown in Paper III. The repeat observations compare favorably. The high ion lines of C IV and Si IV are strong. Even though blending with the SMC features is a problem, these lines definitely have less extension to positive velocities than do their LMC counterparts. Galactic N V is not detected with an upper limit of 30 mÅ for the λ1242.80 line. Different ions exhibit different line profiles. This is best illustrated by comparing the mean absorption velocity of lines of different ions. For example, the well observed species Fe II, Si II, Si IV, and C IV have average absorption velocities of −9, 0, 4, and 10

km s^{-1} respectively. Such differences occur in other ions as well. The limited velocity range over which absorption occurs hampers the recognition of different cloud components in the Milky Way part of the profile. Components near 85 and 300 km s^{-1} have been attributed to SMC gas (see Paper III) although a Milky Way origin is possible.

V. THE LOCAL INTERSTELLAR MEDIUM TOWARD THE MAGELLANIC CLOUDS

We are primarily interested in using the observations reported in this paper to obtain new information about the physical conditions of the Milky Way gaseous halo, here defined as the galactic region with $|z| \gtrsim 1$ kpc. The galactic latitudes of the LMC and SMC at $-33°$ and $-45°$ are such that the lines of sight extend mainly through the halo region. However, all the lines of sight also sample disk material in the solar vicinity. Information on this disk material can be inferred from the 21 cm emission profiles in the directions of six of the Magellanic Cloud stars measured by Koornneef and McGee (1981). The profiles were obtained with the Parkes 64 m telescope with a half-power beamwidth of 15′, and the data for HD 36402 are shown in Figure 3. The gas producing the 21 cm emission near $v_{LSR} = 0$ km s^{-1} is presumably local disk gas. The H I column densities from Koornneef and McGee (1981) for the galactic part of the profile and assuming no self absorption are given in Table 1. The range in N(H I) from 3.5 to 5.5×10^{20} atoms cm^{-2} suggests an equivalent range in $E(B-V)$ from 0.06 to 0.10 based on the average solar vicinity gas-to-reddening ratio of Bohlin, Savage, and Drake (1978). The 21 cm emission profiles of Koornneef and McGee do not exhibit intermediate or high velocity components except for those components obviously associated with Magellanic Cloud gas. In contrast, the C II absorption line profiles shown in Figure 2*f* exhibit an enormous velocity extent because of their high sensitivity for low column density gas.

Additional information about the local interstellar medium in the direction of the Magellanic Clouds has been obtained from the *IUE* spectra for the two Galactic stars listed at the bottom of Table 1. Assuming main sequence luminosities and the color excesses as given in Table 1, we find that these stars lie at ~900 pc. If these stars are subluminous, the distance estimates will need modification. In any case, the path toward the Galactic stars only samples relatively nearby gas. We will not give a detailed discussion of the interstellar line spectra of these two stars; the situation is confused by the fact that both stars have a relatively small rotational velocity and therefore show a rich stellar spectrum. The essential aspects of the interstellar spectra that are of importance for this paper are:

1. The high ion interstellar lines of C IV and Si IV are at most marginally detected (see Table 3). This is in marked contrast to the large equivalent widths for these ions listed in Table 2 for the distant Magellanic Cloud stars.

2. For HD 33599 which is in the direction of the LMC, the low ionization lines which are severely contaminated by stellar absorption show only a limited velocity extent. The best example is the O I λ1302.17 line for which we infer $v_+ \approx 35$ km s^{-1} which is ~100 km s^{-1} smaller than the entries for the LMC stars in Table 2.

From searches in the radio, optical, ultraviolet, X-ray, and γ-ray literature we were unable to find any information that suggests that the local or distant Milky Way interstellar medium toward the Magellanic Cloud stars of this study is atypical. Of particular importance is the fact that the soft X-ray maps of Sanders *et al.* (1977) do not show peculiar emission enhancements in these directions. The nearest pronounced soft X-ray enhancements are in the Vela region, a full 30° from the direction being studied. We believe that the interstellar lines of sight sampled in this study probably pass through normal disk and halo gas. At the distances of the Magellanic Clouds, gas in the Magellanic Stream (Mathewson, Schwarz, and Murray 1977) may influence our observations. However, this gas appears to have radial velocities that will cause its absorption to blend with the Magellanic Cloud part of the ultraviolet absorption profiles.

TABLE 3

IUE OBSERVATIONS OF GALACTIC STARS IN THE DIRECTIONS OF THE LMC AND SMC

				W_λ(Si IV) (mÅ)		W_λ(C IV) (mÅ)	
STAR	l	b	d(pc)	λ1402.77	λ1393.76	λ1550.77	λ1548.20
HD 33599...	271.3	−35.9	~900	<40	<50	<60	<50
HD 10747...	298.9	−41.1	~900	[a]	[a]	80[b]	70[b]

[a] The stellar blending is severe; it is not possible to obtain a useful measurement of the interstellar component.

[b] The stellar spectrum in this wavelength region is complex; these measurements may refer to a combination of stellar and interstellar absorption and therefore should be regarded as upper limits.

VI. EVIDENCE FOR GAS IN THE HALO OF THE MILKY WAY

The ultraviolet spectra discussed in § III and IV contain strong evidence for the widespread existence of gas with $|z| \gtrsim 1$ kpc. Detailed discussions of this evidence are threaded throughout the following sections of this paper. However, a summary of the evidence serves as a useful introduction to the comprehensive discussions to follow. The principal evidence is:

1. Since nearby Galactic stars usually exhibit relatively weak lines of C IV and Si IV (see Papers I and III), the great strength of these lines toward the LMC and SMC stars is probably produced by absorption from gas with $|z| \gtrsim 1$ kpc. This conclusion is further strengthened by the weakness of the C IV and Si IV lines toward the Galactic stars HD 33599 and HD 10747 (see § V).

2. The enormous velocity extension of the strong low ion lines toward LMC stars and the smaller velocity extension toward SMC stars is most easily explained by the effects of differential galactic rotation of gas in a corotating galactic halo, provided the halo gas exists out to distances of about $|z| \approx 10$ kpc. The low ion lines toward the galactic star HD 33599 (see § V) imply that the high-velocity low ion gas toward LMC stars must be more distant than $|z| \approx 0.5$ kpc.

VII. VELOCITIES AND GALACTIC ROTATION

The absorption lines we have detected are very strong, and toward the LMC stars many of the lines are exceedingly wide. For example, toward HD 36402, C II λ1334.53 has an equivalent width of 970 mÅ and a full width at half-absorption of 225 km s^{-1}. In contrast, strong interstellar lines of abundant elements toward Galactic stars with distances less than about 2 kpc usually have full widths at half-absorption of less than $\sim$70 km s^{-1} (Cowie and York 1978). With such a large extent in the absorption profiles, the most straightforward interpretation is that we see the effects of differential galactic motions, which in the directions we are probing mainly produces a positive velocity extension to the absorption.

Knowledge of the rotation of the Galaxy is essentially limited to the region within the solar circle. Even there considerable revisions have been made since the rotation curve and galactic model of Schmidt (1965), which we used in Paper I. Gunn, Knapp, and Tremaine (1979) have rederived the rotational constants of our Galaxy from the available 21 cm surveys. Their result, adopting the revised distance of the Sun to the center of the Galaxy (Oort and Plaut 1975 and references therein), indicates a rotational velocity of the H I gas which is approximately constant at 220 km s^{-1} for $4 < R < 9$ kpc. Beyond the solar circle, one may add to the 21 cm rotation curve, velocities derived from CO emission associated with H II regions (Blitz 1979). Recalculating his data with the constants of galactic rotation found by Gunn, Knapp, and Tremaine, indicates a smooth extension of the rotation curve out to 13 kpc near the 220 km s^{-1} level. We therefore will adopt that the rotational speed of our Galaxy is constant for all $R > 4$ kpc at 220 km s^{-1}. A flat rotation curve is in agreement with what is observed in other spiral galaxies (Bosma 1978; see Faber and Gallagher 1979).

Gas at large distances away from the plane of the Galaxy must participate somehow in the rotation of the plane of the Galaxy. Weisheit (1978) has summarized the theoretical arguments that favor corotation of a gaseous halo. Corotation may occur since the galactic magnetic field that extends into the halo is probably attached to disk gas. The field will therefore attempt to follow the rotational motions of the disk and may drag along ionized halo gas. Observational support for corotation up to $|z|$ distances of 1 to 2 kpc comes from the 21 cm emission measurements of Kepner (1970). Additional, but weaker, support comes from the limits to the anisotropy of cosmic radiation within the energy range of $10^{12} - 10^{14}$ eV, suggesting a local streaming velocity of cosmic rays of less than 100 km s^{-1} (Osborne 1975), hence possibly indicating corotation of the magnetic field in the halo.

Peculiar motions may also exist. Supernova explosions in or near the galactic disk can produce extensive gaseous regions with organized motions. Hot gas in the disk will be buoyant and will attempt to flow toward larger $|z|$. This gas may cool, condense into clouds, and fall back toward the plane (Shapiro and Field 1976). The motions that arise in such a "galactic fountain" have been considered by Bregman (1980). Other phenomena may also occur. For example, halo gas may participate in those processes that create and destroy spiral arms. Perhaps the twisting of magnetic field lines in the halo leads to galactic flares (Sturrock and Stern 1980) and a complex pattern of motions. Further, the galaxy might have a wind, or matter might fall in from intergalactic space. Nevertheless, in spite of all these complications, it appears probable that the overall velocities of the gas at $|z| \approx 1-5$ kpc will to a first approximation reflect the differential rotation of material in the galactic disk. In the following discussion we will adhere to that picture but where needed will consider the consequences of peculiar motions.

Proceeding to the observations, we have summarized the velocity information in the form of a bar chart (Fig. 4) similar to the one shown in Paper III. Rather than judge in a somewhat subjective way the extent of the absorption from the collection of lines available (as in Paper III) we have here used specific ions to describe the absorption extents at half intensity (see Fig. 4 caption). The dots in the bars for the moderately strong low ions represent the central velocities of absorption components. The bars for the high ions exclusively are based on Si IV and C IV. At the top of Figure 4 we have

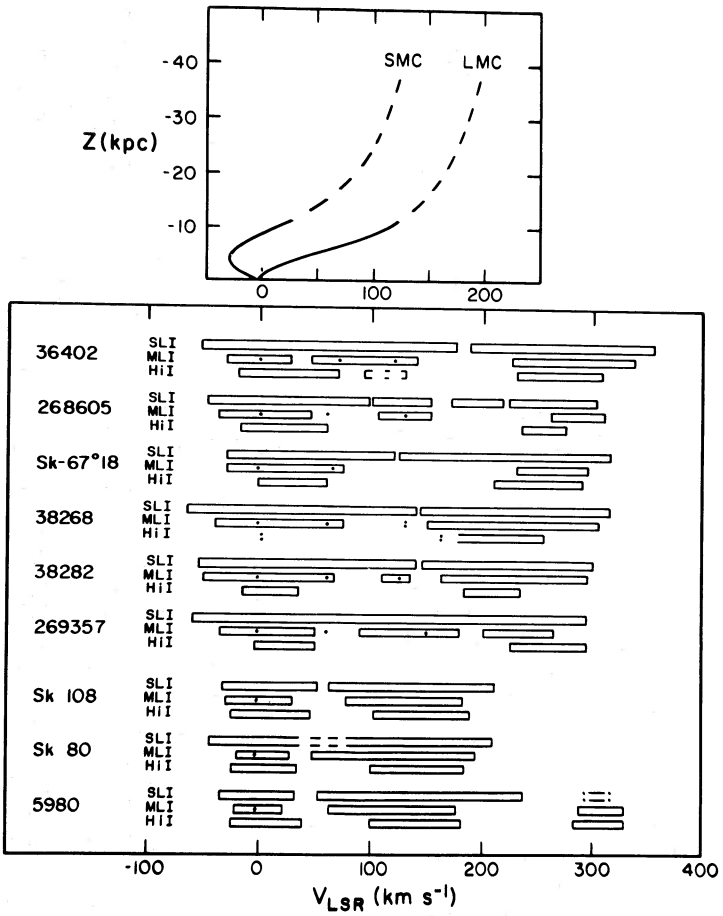

FIG. 4.—Half-intensity velocity extent of the absorption seen in the indicated species in the spectra obtained; SLI = strong low ion, C II λ1334.53 from Table 2; MLI = moderately strong low ion, average of Si II λ1304.37 and Al II λ1670.79 from Table 2, and the dots are the central velocities for the absorption components detected (see Table 4) in the weaker low ion lines; Hi I = high ions, the average from available data of the Si IV and C IV lines. Colons denote absorption with uncertain extent. The stars are arranged according to galactic longitude, hence the three lowest are in the SMC. At the top of the figure we have sketched the radial velocities expected along each line of sight as a function of z, assuming a corotating halo with $\theta = 220$ km s^{-1} for $R > 4$ kpc as discussed in § VII. The validity of the corotation assumption becomes more and more questionable as z increases. Therefore the extensions of these curves to very large z are indicated with dashed lines.

sketched those radial velocities one would expect at different z along our lines of sight if the halo gas corotates with the disk. For the directions to each Magellanic Cloud only one curve is given because differences for paths within 3° of each other are insignificant.

From the bars it is evident that toward the LMC stars the absorptions are wider (extend to more positive velocities) than to the SMC stars, in agreement with that expected from galactic rotation. The average highest velocity to LMC stars is $\langle v_+ \rangle_{C\,II} \approx 150$ km s^{-1}, while to the SMC it is $\langle v_+ \rangle_{C\,II} \approx 50$ km s^{-1}. Presumably, the effects of random cloud motions and instrumental broadening affect the interstellar profiles toward the LMC and SMC in a similar way. Hence, these effects may cancel when considering the 100 km s^{-1} *difference* in velocity extent toward the LMC versus SMC. If this C II absorption is due to corotating halo gas in the directions of each Magellanic Cloud, the difference in the maximum velocity extent suggests that the high-velocity absorbing material is located at $|z|$ distances of up to about 10 or 15 kpc (see the rotation curves of Fig. 4).

To the negative velocity side, the extent of the LMC and SMC absorption features are similar even though the rotation curve in the direction of the SMC reaches velocities 30 km s^{-1} more negative than anywhere along the path to the LMC. Galactic rotation velocity differences smaller than ~30 km s^{-1} may be masked by the effects of random cloud motions. Furthermore, if the line of sight gas distribution is patchy, then the full differential rotation effects may not be seen in a line profile.

At closer inspection we find in the LMC spectra of the low ions discrete absorption components (see Table 4). Easily recognizable is a component near 130 km s^{-1}

TABLE 4

SOME RADIAL VELOCITIES (km s^{-1} LSR) FOR THE INTERSTELLAR MEDIUM TOWARD THE MAGELLANIC CLOUDS

Star	l	b	$\langle v \rangle$ for Galactic 21 cm Emission[a]	Central Velocities for Intermediate and High Velocity UV Components		Limiting Velocities (v_-, v_+) for C II λ1334.53	
HD 36402.....	277.8	−33.0	−1	70	120	−52	175
HD 268605.....	278.9	−36.3	−1	60	130	−47	153
Sk −67°18.....	278.2	−36.0	−2[b]	65	...	−70	120
HD 38268.....	279.4	−31.7	−3	60	130:	−65	140
HD 38282.....	279.4	−31.7	−3	60	125	−56	134
HD 269357.....	279.9	−33.4	−3[c]	60	140	−61	185[d]
Sk 108.....	301.6	−45.0	−2	...	...	−33	50[e]
Sk 80.....	302.1	−45.0	−2	...	...	−40	40[e]
HD 5980.....	302.1	−44.9	−2	...	...	−35	40

[a] These average galactic 21 cm emission velocities are from the measurements of Koornneef and McGee 1981.
[b] This velocity is from the nearby star Sk −67°14.
[c] This velocity is interpolated from the Koornneef and McGee 1981 data for nearby stars.
[d] Inferred from Si II; the galactic and LMC C II blend together.
[e] Inferred from C IV; the galactic and SMC C II blend together.

(in all but one LMC star spectrum), and another near 60 km s^{-1} is indicated in all LMC spectra but can be recognized only in the relatively weak absorption lines. In the SMC spectra all velocities pertaining to the Galaxy blend so much that component structure is not evident, except possibly in the Fe II lines in the long wavelength spectrum of HD 5980.

We have searched the literature for 21 cm data in the observed directions, but published data are scarce and the existing measurements frequently do not have the necessary sensitivity to reveal low column density high-velocity clouds. The 21 cm profiles of Koornneef and McGee (1981) do not reveal any structure at the positive velocities where we have detected the ultraviolet components. In the plane of the Galaxy near $l=280°$ Hindman and Kerr (1970) detected emissions at positive velocities +70 km s^{-1} near $b=-1.5°$ and at +100 km s^{-1} near $b=-4°$, probably due to distant spiral arms which tend to show up at slightly negative latitudes. Goniadzky and Jech (1970) mapped H I down to $b=-15°$, and they find that the velocity component at +90 km s^{-1} extends down to $-14°$ with a gradual change in velocity to +60 km s^{-1}. Such extensions also have been detected elsewhere in the Galaxy and have been attributed to warping of the galactic plane and/or considerable z extension of spiral arms (Kepner 1970; Verschuur 1973*b*). At positive latitudes $b>10°$ near $l=280°$ Wannier, Wrixon, and Wilson (1972) detected several clouds with velocities between +60 and +250 km s^{-1}.

The material we detect at +60 km s^{-1} may constitute a high-z extension of a spiral arm. The velocity, together with the rotation curve of Figure 4, indicates a line of sight distance of ~13 kpc or $z\approx-7$ kpc, although a larger distance would be indicated if this cloud is the extension away from the plane of the Galaxy in H I seen at +90 km s^{-1} by Goniadzky and Jech (1970). Its location could be compared with the approximate location of spiral arms sketched by Verschuur (1973*a*).

The material detected at +130 km s^{-1} similarly would be at a line of sight distance of 30 kpc and $z\approx-15$ kpc, hence a projected distance from the galactic center of ~25 kpc. At a distance ~15 kpc away from the plane of the Galaxy it is hard to imagine that this material is a high-z extension of a spiral arm. At such large z distances the corotation assumption will very likely become invalid and, as indicated above, it very well may be that peculiar motions are involved. It is remarkable that we see absorption near +130 km s^{-1} over an area at least as large as 7 square degrees. The lateral extent of the absorbing gas would be at least 2 kpc (if at 30 kpc distance) and with N(H I) between 5×10^{18} and 2×10^{19} cm^{-2} (see § VIII) the total mass would be greater than 3×10^5 $M_\odot$. This component at +130 km s^{-1} very well may be a low-column-density extended high-velocity cloud of the kind discussed by Hulsbosch (1975).

Finally, we remark that if the detected clouds have a velocity perpendicular to the plane of the Galaxy of 40 km s^{-1} (either way), that velocity has a component of 20 km s^{-1} along the LMC line of sight, and of 28 km s^{-1} along the SMC line of sight. From Figure 4 (*top*) one can then infer how much the distance estimates may be affected.

VIII. LINES OF LOW IONIZATION SPECIES AND ABUNDANCES

It is of considerable interest to investigate the composition of the gas detected at high velocities in the halo. Information on relative element abundances might provide clues about the origin of the gas, while information about relative ionic abundances is important for inferring the physical conditions within the gas.

In principle, the observed line strengths may be used to find column densities. However, the use of a curve-of-growth procedure is a risky venture because velocity blending of different absorbing clouds produces a total absorption curve of growth that is a complex blend of simple curves of growth. In short, the absorption lines from different elements may follow different curves of growth depending on (1) the severity of the blending, (2) the cloud to cloud variations in the gas-phase relative abundances, and (3) the state of ionization of the halo gas. In some cases (e.g., for Fe II) we have observed many lines with a large range of f-values, and reliable column densities can be inferred from the data. In other cases (e.g., O I, C II, Al II, Si III) only one strong line is available and therefore we can usually only place limits on the column densities. For Si II we have a number of lines, but the uncertainty in the f-values (see York and Kinahan 1979) limits our analysis (see note added in proof).

Galactic rotation produces less separation of disk and halo absorption in the direction of the SMC. Therefore our emphasis will be on the LMC data.

Figure 5 shows the character of the absorption line strengths toward HD 36402, the best observed LMC star. In Figure 5*a* (*lower panel*) the total absorption strength log W_λ/λ is plotted against log $(Ab_\odot f\lambda)$, where $Ab_\odot = 10^{12}[X/H]$ corrects the data to a solar abundance scale. If all the elements along the line of sight had both solar relative abundances and the same curve of growth, then plots of the type produced should be smooth. Deviations would indicate abundances differing from solar abundances, or deviations produced by ionization effects, or deviations produced by blending effects. The solar abundances used in producing Figure 5 and listed in the legend were taken from the updated compilation of Ross and Aller (1976). Lines from ion states which are dominant in the general interstellar medium have been plotted. Lines of lower

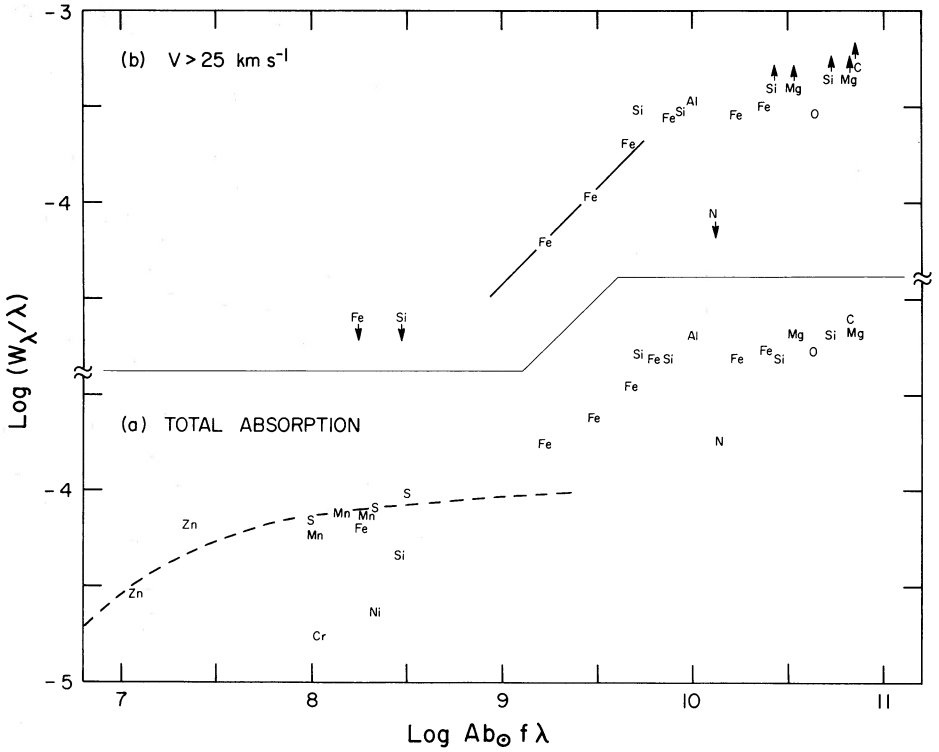

FIG. 5.—Absorption strength log W_λ/λ versus log $(Ab_\odot f\lambda)$ for galactic interstellar absorption toward HD 36402. Fig. 5*a* illustrates total absorption over the range of galactic velocities -60 km s^{-1} to $+175$ km s^{-1}; Fig. 5*b* shows absorption strengths for the high velocity absorption, $+25$ km s^{-1} to $+175$ km s^{-1} only. $Ab_\odot \equiv 10^{12}$ $(X/H)_\odot$ adjusts the data to solar abundances on the line of sight. Deviations from a smooth curve are expected as discussed in the text. The ions plotted with their element symbol include C II, N I, O I, Mg II, Al II, Si II, S II, Cr II, Mn II, Fe II, Ni II, and Zn II. The Zn II lines establish the absolute scale in Fig. 5*a*; a theoretical unsaturated line has log $W_\lambda/\lambda = -4.5$ at log $Nf\lambda = 15.55$. Fig. 5*a* shows that for this enormous line of sight no single cloud curve of growth will fit. The dashed curve is a simple Doppler broadened curve for $b = 8$ km s^{-1}. The rise indicated by the Fe II and Si II lines near log $Ab_\odot f\lambda = 9.5$ is due to the increasing contribution of the high-velocity clouds to the total absorption, yet their column densities are at most 6% of the column density found for the $v \approx 0$ km s^{-1} gas. In Fig. 5*b* the weaker Fe II lines are well described by the linear curve of growth illustrated. The following logarithmic abundances from Ross and Aller (1976) were used making the figure: H = 12.00, C = 8.62, N = 7.94, O = 8.84, Mg = 7.60, Al = 6.25, Si = 7.65, S = 7.20, Cr = 5.71, Mn = 5.42, Fe = 7.50, Ni = 6.28, and Zn = 4.45.

and higher ion stages would be expected to behave differently from those plotted (see § IX). Figure 5*b* (*upper panel*) illustrates line strengths toward HD 36402 in the high velocity gas ($v > 25$ km s^{-1}).

a) High-Velocity Clouds in the Direction of the LMC

In most of the LMC star spectra we can resolve the absorption due to the high velocity cloud near 130 km s^{-1} from the lower velocity absorption. In HD 36402 the clouds at 70 and 120 km s^{-1} together can be separated from the absorption near 0 km s^{-1}.

The fairly large number of Fe II lines in HD 36402, detected at velocities greater than 25 km s^{-1}, establishes an empirical curve of growth which, although from a blend of two high velocity clouds, closely follows a single-cloud curve of growth (see Fig. 5*b*). From the shape of the Fe II curve it is clear that the weakest Fe II lines must be unsaturated, and so log N(Fe II) = 14.4 ± 0.1.

The entries for C II, Mg II, and two of Si II are lower limits due to the blend with absorption near $v = 0$ km s^{-1}. The plotted line strengths, however, must be close to the real values because they represent essentially total absorption between +25 km s^{-1} at the low velocity side, and v_+. For these high velocity absorptions, the strong Fe II, Si II, and Mg II lines seem to establish the flat part of the empirical curve of growth. But difficulties may arise, as mentioned, with the use of one curve for these species. However, Si, Fe, and Mg have essentially the same abundance in the Sun, presumably could be depleted into dust in comparable amounts, have similar high ionization potentials, but differ in the dielectronic recombination which starts at log $T_e \sim 4.3$, 4.0, and 3.8, respectively. Mg II, in particular, may have absorption from high temperature gas, but from the observations it appears that the Mg II and Si II lines are of almost equal strength. In short, if the use of one curve of growth is valid, Fe, Mg, Si, and also Al appear with abundance ratios near the solar values. Being conservative, we must give for Si II, Al II, and Mg II only lower limits to the column density based on the strength of the weakest detected line; these are log N(Si II) ≥ 14.5, log N(Al II) ≥ 13.1, and log N(Mg II) ≥ 13.8.

Neutral oxygen, representing strictly neutral gas, also has only one line in our spectra. That line is relatively weak at the high velocities, and it is below the Fe II, Si II, and Mg II data points in Figure 5*b*. That may be due to the fact that absorption by the latter ions also occurs in ionized gas. On the other hand, the oxygen point may be on a flat extension of a curve of growth established by the Fe II data. Referring the oxygen absorption to that curve, the column density could be as large as log N(O I) = 15.5, but only the lower limit based on no saturation at all, log N(O I) > 14.7 is trustworthy.

Neutral nitrogen is not clearly detected at high velocities in our HD 36402 spectra. Although the lines of N I are in a part of the spectrum with low instrumental sensitivity, we have quoted a conservative upper limit for the line strength in Table 2. The upper limit suggests a N/O ratio smaller than in the Sun. This could indicate that N is deficient, a result also of importance for the fact that N V is undetected in our spectra while other high ions have strong lines (see § IX). Higher quality measurements will be needed to conclusively establish this apparent abundance anomaly.

The two high velocity clouds in HD 36402 also can be resolved from each other in most of the Fe II lines (see Fe II λ2599.40 in Fig. 2*b*). The absorption at 70 km s^{-1} is only slightly weaker than at 120 km s^{-1}. With an approximate decomposition for the stronger lines we were able to construct two curves of growth that resemble simple Doppler curves of growth with $b = 10$ km s^{-1}. The separated column densities are listed in Table 5. The fact that these two high-velocity clouds have almost equal column density and similar b-values justifies the use of the single curve of growth of Figure 5*b* (for discussion of blends see Nachman and Hobbs 1973).

Toward the other LMC stars the decomposition of the absorption profiles in the components near 0, 60,

TABLE 5

FE II COLUMN DENSITIES LOG N(cm^{-2}) IN HIGH-VELOCITY CLOUDS

STAR	$b°$	COMPONENT +60 km s^{-1}	COMPONENT +130 km s^{-1}	FROM TOTAL ABSORPTION[a]
HD 38282	−31.7	13.6	13.5	13.8
HD 36402	−33.0	14.0	14.1	14.4
HD 268605	−36.3	13.7	13.8	14.0

[a] Independent determination; the total is more reliable than the sum from the two individual clouds.

and 130 km s^{-1} is less obvious. For most spectra, the 60 km s^{-1} absorption is stronger than the 130 km s^{-1} absorption, and the 60 km s^{-1} feature severely blends with the absorption near 0 km s^{-1}. In some spectra a rough separation could be made. In most cases the 130 km s^{-1} cloud can be treated independently. However, these remarks essentially refer to Fe II only. The other species either have too few lines to be used or the blending is too severe to trust an interpretation toward a column density. Those column densities that could be inferred for the high-velocity material toward the LMC stars are listed in Table 5.

The data of Blades (1980) toward HD 38268 show interstellar Ca II components near +50 and +130 km s^{-1}, and from the strengths we deduce that log N(Ca II)$\approx$11.6 and 11.4, respectively. If Ca II is present with solar abundances, these clouds would have a total log N(H)$\approx$17.5, but then we ignore a quite uncertain correction for the ionization structure (a considerable amount of calcium could be Ca III) and the possible depletion (Ca is among the elements with very strong depletion in the galactic plane).

b) *Low Velocity Absorption the Direction of the LMC*

In the spectrum of HD 36402, the absorption centered near 0 km s^{-1} can easily be separated from the total absorption. Zn II and S II are two elements that exhibit very little depletion in the local interstellar medium (for a review see Savage and Mathis 1979). Toward HD 36402 these species only show absorption by the gas near 0 km s^{-1}. From the strengths of the Zn II lines it follows that log N(Zn II) = 13.0 $\pm$ 0.2. Comparing this to the 21 cm galactic column density from Table 1, we find log (Zn/H) = -7.73 ± 0.2 in good agreement with the solar abundance ratio of log (Zn/H) = -7.6 (Ross and Aller 1976). Assuming solar abundances for S II as well, the Zn and S II data suggest a curve of growth for the $v = 0$ km s^{-1} gas close to a simple Doppler broadened curve with $b = 8$ km s^{-1}. With this curve of growth, the column densities and depletions for HD 36402 listed in Table 6 are obtained. Results for species like C II, O I, and Al II are not reported since only one strong and severely blended line is available.

Table 6 also lists the column densities and depletions found toward other LMC stars from the low velocity absorptions through a procedure similar to that used for HD 36402. For comparison purposes we also list in Table 6 the average depletion found for these species from existing studies of disk gas.

c) *Absorption in the Direction of the SMC*

Toward the SMC the absorption near 0 km s^{-1} is strong. Additional components with $v > 80$ km s^{-1} are not clearly distinguished in the profiles. If galactic components with $v > 80$ km s^{-1} exist, they will blend with the SMC interstellar lines. We therefore will only discuss the total absorption line strengths for gas near 0 km s^{-1} which mainly provides information on gas in the solar vicinity.

For Zn II we find log N(Zn II) = 13.0 $\pm$ 0.2 toward Sk 80 and Sk 108, and log N(Zn II) = 12.8 $\pm$ 0.2 toward HD 5980. Assuming no depletion and solar abundances, these numbers imply log N(H I) = 20.5, which is close to the 21 cm H I emission column densities of Table 1. Toward these stars S II also follows simple Doppler broadened curves of growth based on solar abundances. With the Zn II–S II curves of growth we then obtain the results for Mn II, Ni II, and Cr II listed in Table 6. A smooth extension of the Zn II–S II curve of growth is found for all the other species, but the noise in the data and flatness of the curve prevent us from obtaining additional reliable column densities.

Absorption from the excited level of ionized carbon, C II*, is detected near galactic velocities in the spectra

TABLE 6

DEPLETIONS, LOG(X/H) − LOG(X/H)$_\odot$ IN GAS ABSORBING NEAR 0 km s^{-1}

Star	Cr	Mn	Fe	Ni	Zn
HD 36402....	−1.4	−0.4	−0.8	−1.5	−0.1
HD 268605...	< −1.2	−0.6	−1.0	−1.5	+0.1
Sk −67°18...	< −1.2	d	d	−1.4	0.0
HD 38282....	−1.2	−0.7	−0.3:	−1.2	−0.1
HD 269357...	< −1.2	d	d	−1.4	0.0
HD 5980.....	−0.8:	−1.0	e	−1.3	0.0
Average....	$\lesssim$ −1.2	−0.7	−0.8	−1.4	0.0
Galactic....	−1.6:[a]	−0.80[b]	−1.84[c]	−2.0:[a]	0.0[a]

[a] Averages from Morton 1975, 1978, corrected for revised f-values.
[b] De Boer and Lamers 1978, adjusted to Fe depletion of Savage and Bohlin (1979).
[c] Savage and Bohlin 1979, adjusted to adopted solar abundance.
[d] No long wavelength ultraviolet data obtained.
[e] Not measurable due to curve-of-growth problems.

of SMC stars. Toward the LMC, however, the LMC absorption of C II usually blends with the possible Galactic C II* absorption. The C II* lines measured have strengths very common for galactic lines of sight (see, e.g., Morton 1978) although there the C II line usually is only slightly stronger than the C II* line. Our spectra indicate that C II is 3 times as strong, which is probably due to sampling of very extended lower density gas.

d) *Discussion*

In the high-velocity clouds in front of the LMC stars, the detection of oxygen signifies a considerable amount of neutral gas. In particular for HD 36402 from the lower limit, log N(O I) $\geq$ 14.7, we find log N(H I) $\geq$ 17.9 if oxygen has a solar abundance. This limit for H I would be increased if oxygen at large z is underabundant. For the heavy metals: log N(Fe II) = 14.4, log N(Mg II) $\gtrsim$ 13.8, log N(Al II) $\geq$ 13.1, and log N(Si II) $\gtrsim$ 14.5. If these ions exist on our lines of sight in neutral gas alone, the respective values of log N(H) are 18.9, $>$ 18.2, $>$ 18.6, and $>$ 18.9, based on solar abundances. The existing 21 cm profiles unfortunately fall short in sensitivity to provide a meaningful comparison column density. In the profiles of Koornneef and McGee (1981), one of which is illustrated in Figure 3, there is a hint of a component near +60 km s^{-1} toward HD 36402 but the +130 km s^{-1} component is not apparent. This is similar to several high-velocity clouds which are seen in metals (Ca II, Na I) but not in H I (see Habing 1969). From these data and the assumption FWHM $\approx$ 20 km s^{-1} we can only place the limit, log N(H I) $\lesssim$ 19.2 for each high-velocity component.

Pending the availability of 21 cm data highly sensitive in N(H), our conclusions on abundances toward HD 36402 are limits: (*a*) the neutral high-velocity clouds contain oxygen with an abundance larger than 3% of the solar abundance; (*b*) if (for simplicity) all the detected Fe II, Si II, Al II, and Mg II is in neutral gas, these elements have abundances in the high-velocity clouds of *at least* 5–25% of the solar abundance, but any fraction of ionized gas sampled on the line of sight would lower these numbers in that proportion; (*c*) nitrogen possibly is deficient compared with oxygen, but confirmation from higher quality data is needed; (*d*) the line from C II, which samples both neutral and ionized (up to 24.4 eV) gas, down to detectable absorptions from column densities of H + H$^+$ as small as 2×10^{17} cm^{-2}, indicates the presence of gas at velocities as large as $\sim$170 km s^{-1}; (*e*) with the detection of these metals which may be present with abundances within an order of magnitude of solar abundances, we clearly have probed chemically processed gas away from the plane of the galaxy; (*f*) the mass of these clouds (see § VII) may exceed 3×10^5 $M_\odot$.

In the $v = 0$ km s^{-1} gas we have determined abundances for Zn II, Mn II, and Fe II, and, from single absorption lines only, for Cr II and Ni II. These may be compared with results for gas in the Galaxy from earlier studies (see Table 6). The significant difference is that we obtain for Fe II a depletion a factor 10 less severe than in gas in the plane of the Galaxy. Shull, York, and Hobbs (1977) have found that in high-velocity clouds, at distances of several hundred parsec, Fe II also has nearly solar abundance. It may well be that the gas we sampled in the first few kiloparsecs of the lines of sight to the Magellanic clouds partly resembles such locally detected high-velocity gas.

IX. LINES OF HIGHLY IONIZED SPECIES

The high ionization lines of Si IV and C IV detected at galactic velocities are exceptionally strong toward all the Magellanic Cloud stars. In contrast, N V is not detected, with best case upper limits at the 30 mÅ level for the λ1242.80 line. Because Si III and C III ionize at 33.5 and 47.9 eV, respectively, (N V would exist between 77.5 and 97.9 eV), the presence of strong lines of Si IV and C IV suggests the widespread existence of hot gas. If the ionization is from electron collisions balanced by radiative and dielectronic recombination, then Si IV, C IV, and N V peak in abundance at 0.65, 1.1, and 1.9×10^5 K, respectively (Shapiro and Moore 1976; Baliunas and Butler 1980). Thus, temperatures around 10^5 K are implied. However, other ionization mechanisms may be operative, and the assumption of time equilibrium is questionable (see § X). Conclusions about gas temperatures should therefore be treated with caution. The detection of these lines at galactic velocities in the spectra of extragalactic objects provides definitive proof that highly ionized species exist in the general interstellar medium of our Galaxy away from local stellar environments. The detections of Si IV and C IV at zero redshift in low-resolution *IUE* spectra of 3C 273 (Ulrich *et al.* 1980) at $l = 289°$ and $b = +64°$ gives additional evidence for the global galactic existence of these ions.

In Table 7 the average high ion line strengths toward LMC and SMC stars are given along with values for HD 36402 in the LMC and HD 5980 in the SMC, the two best observed stars. The Si IV and C IV equivalent widths are $\sim$2 to 4 times larger than those observed toward Galactic field stars which are not associated with nebulosity and which are at distances less than $\sim$2 kpc (see Bruhweiler, Kondo, and McCluskey 1980; Black *et al.* 1980). In addition, the lines are $\sim$4 times stronger than the upper limits for the two Galactic stars we observed in the direction of the LMC and SMC at $r \sim 0.9$ kpc (see § V and Table 3). The great strength of these lines toward the Magellanic Clouds is probably produced by gas beyond $r \sim 0.9$ kpc. The positive velocity extension of the Si IV and C IV lines toward the LMC suggests that the absorption may be produced by gas with $|z|$ distances up to about 10 or 15 kpc (see § VII and Fig. 4).

TABLE 7

HIGH ION LINES TOWARD MAGELLANIC CLOUD STARS

OBJECT	Si IV(W_λ in mÅ) λ1402.77	λ1393.76	DR[a]	log N(Si IV)
HD 36402 .	140:	240	1.7:	~13.5
⟨LMC⟩[b]...	130	230	1.7	~13.5
HD 5980 ..	150	190	1.3	~13.8
⟨SMC⟩[b]...	180	210	1.2	~13.8
	C IV (W_λ in mÅ) λ1550.77	λ1548.20	DR	log N(C IV)
HD 36402 .	220	400	1.8	~14.0
⟨LMC⟩[b]...	190	350	1.8	~13.9
HD 5980 ..	330	330	1.0	>14.3
⟨SMC⟩[b]...	310	340	1.1	>14.3
	N V (W_λ in mÅ) λ1242.80	λ1238.20		log N(N V)
HD 36402 .	<30	n[c]	...	<13.5
HD 5980 ..	<30	n	...	<13.5

[a] DR ≡ doublet ratio.

[b] Weighted averages of the LMC and SMC, respectively, high ion equivalent widths.

[c] n ≡ noisy data, measurement omitted.

The doublet ratios of the C IV and Si IV lines listed in Table 7 differ markedly toward the LMC and SMC. Toward the LMC, the line ratios suggest that the absorption lines are hardly affected by saturation. If this is indeed so, the average column densities, with $b > 50$ km s^{-1}, are log N(C IV)≈14.0 and log N(Si IV)≈13.5, and the upper limit for N V assuming no saturation implies log N(N V)≲13.5 (see Table 7). A cautionary remark is needed with these column densities. As Nachman and Hobbs (1973) showed, a cloud with a small velocity dispersion and large column density might contribute negligibly to the absorption line strengths, and the use of just equivalent widths and a doublet ratio could lead to a large underestimate of the actual column density. If the high ion lines represent gas at approximately 10^5 K, the thermal broadening alone would correspond to $b \approx 11$ km s^{-1} for C and $b \approx 8$ km s^{-1} for Si. These velocity dispersions are much smaller than those which follow from the relative line strengths, hence indeed more than one absorbing region must be active on the lines of sight.

Toward the SMC, the doublet ratios are close to unity, implying a considerable amount of line saturation. This result is consistent with that expected from the halo gas corotation assumption, since (see Fig. 4) out to $|z|$ distances as large as about 10 kpc the material toward the SMC would be expected to have a velocity range between only −25 and +25 km s^{-1}. With an assumed b of 15 km s^{-1} the inferred column densities are log N(Si IV)≈13.8, and log N(C IV)≈15.7. Here, however, the simple curve-of-growth procedure cannot be very reliable because of the high degree of saturation, particularly for C IV. The lower limits to the column densities are log N(Si IV)>13.7 and log N(C IV)>14.3. Nevertheless, these limits clearly indicate that toward the SMC the amount of Si IV and C IV is larger than that detected toward the LMC. This may be related to the fact that the SMC line of sight has a projected tangential point at 7.4 kpc from the center of the Galaxy while for the LMC line of sight that projected distance is 8.5 kpc. In the galactic plane near $R \approx 7$ kpc (in the system $R_\odot = 8.5$ kpc) there is a large increase in the density of interstellar particles, H II regions, and supernova remnants (Burton 1976). Perhaps this active inner region of the galaxy can support a denser gaseous halo.

From the column densities of Table 7 and the assumptions of solar abundances and equilibrium electron collisional ionization as calculated by Shapiro and Moore (1976) for C IV and N V and by Baliunas and Butler (1980) for Si IV we can obtain estimates for the high ion gas temperature. Toward the LMC, the value N(C IV)/N(Si IV)≈3 implies $T \approx 0.7 \times 10^5$ K while N(N V)/N(C IV)<0.3 implies $T < 1.5 \times 10^5$ K. Toward the SMC the high degree of line saturation severely limits the accuracy of the column densities and the corresponding T estimates. However, the large apparent ratio of N(C IV)/N(Si IV) would require a temperature in excess of $\sim 10^5$ K but the upper bound is limited by the smaller ratio of N(N V)/N(C IV) to $T < 1.4 \times 10^5$ K. This latter number would of course be invalid if the suspected lower than solar nitrogen abundance discussed in §VIII is correct.

The derived column densities probably refer mostly to the first 10 kpc of the lines of sight. Toward the LMC we then obtain $\langle n(\text{Si IV}) \rangle \approx 1 \times 10^{-9}$ cm^{-3} and $\langle n(\text{C IV}) \rangle \approx 3 \times 10^{-9}$ cm^{-3}, with $\langle n(\text{N V}) \rangle \lesssim 1 \times 10^{-9}$ cm^{-3}. Again assuming collisional ionization at $T \approx 0.7 \times 10^5$ and solar abundances, these numbers imply a total average particle density of $\sim 3 \times 10^{-4}$ cm^{-3}. Toward the SMC the various numbers will be larger by a factor of 2 or more.

The striking difference between the low and high ion line profiles is best illustrated in Figure 3, but other examples can be found in Figure 2 and in Papers I and III. The high ion profiles exhibit a relatively smooth extension to high velocity while the low ion profiles (e.g., Si II and Fe II in Fig. 3) show distinct high and intermediate velocity components. If these profiles are primarily shaped by differential galactic rotation, the difference in smoothness suggests a more uniform line-of-sight distribution of the high ion gas.

In Paper I the asymmetric C IV and Si IV profiles toward HD 38282 were rotationally analyzed, with the assumption of corotating halo gas and the Schmidt (1965) rotation curve, to yield the run of n(C IV) and

n(Si IV) with z distance away from the plane. A similar analysis is shown in Figure 6 for the material toward HD 36402. We again assumed corotation but used a flat rotation curve with $\theta = 220$ km s^{-1} and $R_\odot = 8.5$ kpc (see § VII). The instrumental smearing (FWHM$\approx$ 25 km s^{-1}) was ignored in converting the two-image average C IV and Si IV profiles into the density plot. Of course, the validity of the result depends critically on the assumption of corotation of halo gas. The result for n(C IV) and n(Si IV) suggests that we may have detected halo gas to $z \approx -10$ to -15 kpc along this particular path. The z extent revealed in Figure 6 is larger than found in Paper I since toward HD 36402 we record a higher velocity extension of the high ion lines and since we analyzed the HD 36402 data with a flat rotation law rather than the Schmidt law used for HD 38282. It is clear that while the true extent of this halo gas is very uncertain, the available data suggest numbers in excess of $|z| \approx 10$ kpc.

While the high ion line profiles, toward LMC stars are generally smoother than the low ion lines, there is one case where the high ion data quality is adequate to reveal component structure. Toward HD 36402 the low ion cloud at $v_{LSR} \approx 120$ km s^{-1} is definitely detected in C IV and not detected in Si IV. The C IV equivalent

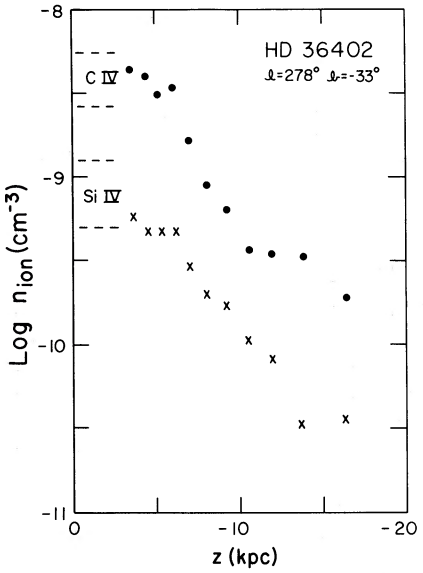

FIG. 6.—C IV and Si IV densities toward HD 36402 as a function of z (distance below the galactic plane). The derived curves assume that the observed velocities in the line profiles represent the radial component of corotating gas in the galactic halo according to the curves of Fig. 4. Due to velocity blending and saturation near $v = 0$ km s^{-1}, the densities between 0 and -3 kpc are only approximate. At very large z the corotation assumption is probably invalid. The presence of gas flows along this particular line of sight would of course invalidate the result. Instrumental smearing was ignored in converting the observed C IV and Si IV profiles into the density distribution illustrated.

widths in this component listed in Table 2 suggest unsaturated absorption and log N(C IV)$\approx$13.2. In comparison, from Table 5 we have in this high velocity cloud log N(Fe II)$\approx$14.1 which, assuming solar abundance ratios, implies log N(C II)$\approx$15.2 and hence N(C IV)/N(C II)$\approx$0.01. Under conditions of collisional ionization this ionic ratio occurs at $T \approx 60{,}000$ K. However, this value of T is not supported by the missing Si IV component at 120 km s^{-1}. A more likely possibility is that the low ion gas and high ion gas do not coexist but the high ion gas is situated in a hotter zone surrounding the cooler low ion cloud (McKee and Ostriker 1977). If the C IV associated with the 120 km s^{-1} absorption is at 10^5 K, the thermal FWHM of the feature would be 20 km s^{-1}, which is slightly smaller than the instrumental resolution (FWHM$\approx$25 km s^{-1}). Unfortunately the uncertain continuum and noisy data make it very difficult to accurately judge the observed width of this feature. However, the relatively sharp line observed (FWHM$\lesssim$40 km s^{-1}) is inconsistent with temperatures in excess of about 3×10^5 K.

X. DISCUSSION

In this section we will attempt to relate the observational results given in earlier sections of this paper to current theoretical ideas about the origin and physical state of gaseous galactic halos. The ultraviolet absorption toward the Magellanic Clouds was broadly characterized as being produced in low ionization gas (§ VIII) and high ionization gas (§ IX). The principal tracers of these gas phases are C II, O I, Mg II, Al II, Si II, and Fe II for the low ion gas, and C IV and Si IV for the high ion gas. The presence of O I absorption at high velocities toward the LMC stars implies that some of the low ion halo gas is neutral even though it is not detected through existing 21 cm emission measurements. The absorption line shapes for the low and high ion halo gas are very different in appearance (see Fig. 3), a result suggesting that we are dealing with *at least* two distinct gas phases.

In the halo gas toward HD 36402 log N(Si II)$\gtrsim$14.5 while log N(Si IV)$\approx$13.5. Therefore, without allowing for other ionization stages such as Si III or Si V, the amount of low ion gas exceeds by about a factor of 10 the amount of high ion gas. Assuming solar abundances, the amount of halo gas detected represents about 2% by mass of that found in the galactic disk.

The fundamental theoretical paper on the expected physical state of gas in galactic halos is that of Spitzer (1956). It was in this paper that the possible existence of a hot ($T \approx 10^6$ K) interstellar corona was first suggested, an idea motivated by the apparent stability of distant high-latitude clouds. The more recent papers on this subject (Shapiro and Field 1976; Weisheit and Collins 1976; Chevalier and Oegerle 1979; Bregman

1980; Sturrock and Stern 1980) represent extensions of many of Spitzer's original ideas.

The wide range of possibilities for the physical state of gas in galactic halos is well summarized by Chevalier and Oegerle (1979). Briefly, the basic ideas are: hot gas ($T \approx 0.3$ to 1×10^6 K) is known to exist in the galactic plane from the measures of soft diffuse X-rays (Sanders *et al.* 1977 and references therein) and from interstellar O VI absorption (Jenkins 1978*a*, *b*). The hot disk gas will be buoyant since gas at $T \approx 10^6$ K will have a scale height in the galactic gravitational field of $\sim$8 kpc (Spitzer 1956). The gas will therefore attempt to flow outward, cool, and perhaps condense into clouds that will fall back toward the galactic disk. Such a "galactic fountain" model was first suggested by Shapiro and Field (1976) and recently examined in detail by Bregman (1980). The rate of cooling and heating of the outflowing gas will determine whether or not a fountain occurs as described above or whether the flow continues outward as a galactic wind. The currently favored view is the fountain model (see Chevalier and Oegerle 1979; Bregman 1980), although, given the limited information about heating mechanisms, other possibilities cannot be ruled out.

Without overstating the correspondence, it appears possible that the low ion gas we are sampling (see § VIII) is related to the condensed material in the galactic fountain model. However, if the infall velocities of this material are large compared to galactic rotation effects, then the distance estimates of § VII will need modification. With the possible exception of N I, the low ion line strengths are consistent with solar relative abundances. Population I abundances would be expected if the gas originates in the galactic disk.

It is not obvious where the high ion gas revealed through C IV and Si IV might fit into the galactic fountain model. If electron collisional ionization balanced by radiative and dielectronic recombinations are responsible for the ionization, then the data suggest gas near 10^5 K, which is cooler than the disk gas that supposedly drives the fountain. Furthermore, 10^5 K is the temperature at which hot ionized gas cools fastest (Raymond, Cox, and Smith 1976); therefore the 10^5 K gas would probably constitute only a small fraction of the gas on our lines of sight.

McKee and Ostriker (1977) have suggested that the conductive interface between cold clouds and hot ($T \approx 10^6$ K) interstellar gas may be responsible for the interstellar O VI absorption observed toward galactic O and B stars. Possible support for this idea is provided by the correlation between the line velocity structures for O VI and those for lower ionization species (Cowie *et al.* 1979). Perhaps the C IV and Si IV we see toward the Magellanic Cloud stars also originates in conductive interfaces. In § IX we noted the presence of a C IV component at 120 km s^{-1} toward HD 36402, a component also detected in the lower ions, but the C IV component was weak and no absorption was obvious in the Si IV lines at that velocity. The apparent overall smoothness of the high ion profiles compared to the low ion profiles (see Fig. 3) suggests to us rather different origins for the low and high ion absorption.

Thus far we have assumed that C IV and Si IV are produced by electron collisional ionization and that the measured column densities can be used to infer gas temperatures. We have no proof that these assumptions are correct, and the *IUE* data quality and resolution make it difficult to obtain temperature information from the line widths. At the very low particle densities toward the Magellanic Clouds one may question the validity of time equilibrium. If the ionization is not balanced by recombination, the true gas temperature and the distribution of the ionization stages will be influenced by the time evolution of the galactic halo gas. In a gas that is cooling from high temperatures, as one would expect in a galactic fountain model, the recombination will lag behind the cooling, and high ionization species might be found in relatively cool gas.

Other mechanisms for high ion production could be ultraviolet or X-ray photon ionization. Depending on the ambient gas densities, ionized regions around hot stars may extend far into the galactic halo (Thuan 1975). Black *et al.* (1980) have shown that the observed column densities of Si III, Si IV, and C IV toward stars located in the galactic disk are in harmony with those expected in normal photoionized nebulae. We note that the average C IV to Si IV column density ratio observed by Black *et al.* is $\sim$0.6 while we observe a ratio of $\sim$3 toward the LMC. The factor of 5 difference would appear to require an ultraviolet photon source much harder than that produced by the 35,000–45,000 K stars included in the Black *et al.* program. The X-rays produced by very hot gas might lead to X-ray Auger ionization of C II and Si II into C IV and Si IV in cool halo clouds. But then the C IV and Si IV profiles should resemble more closely the low ionization counterparts.

The relatively smooth high ion profiles suggest a smooth distribution of the high ion gas on our lines of light. It may be that the Galaxy as a whole has a transition zone between the denser and cooler gas in the plane and the regions in the gaseous halo far out. That very distant gas could be at a temperature of a few million degrees, compatible with the observations of the diffuse soft X-ray flux (Burstein *et al.* 1977; Nousek *et al.* 1980). Such a spatial structure essentially follows the general principles outlined by Spitzer (1956).

Finally, these new data on the galactic gaseous halo provide support to the hypothesis that certain quasar absorption line systems are formed in the gaseous halos of intervening galaxies (Bahcall and Spitzer 1969). In a

separate paper (Savage and Jeske 1981) the present observations will be compared with existing quasar absorption line data.

We express our appreciation to the entire *IUE* staff at the Goddard Space Flight Center for their assistance in acquiring and processing these data. We thank our colleagues at Washburn Observatory and the University of Wisconsin Space Physics Group for numerous discussions. We thank Drs. Koornneef and McGee for providing their H I data before publication. We acknowledge the use of the computer of the Space Astronomy Lab of the University of Wisconsin, and we thank Marilyn R. Meade for assistance with the data handling. We thank Helen Hay and Alice A. Halfen for typing the manuscript and Pam Unguris for her skill in making the figures. This research has been supported by the National Aeronautics and Space Administration under grants NSG 5241 and 5363.

REFERENCES

Abbott, D. C. 1978, *J. Phys. B, Atom. Molec. Phys.*, **11** 3479.
Ardeberg, A., Brunet, J. P., Maurice, E., and Prévot, L. 1972, *Astr. Ap. Suppl.*, **6**, 249.
Bahcall, J. N., and Spitzer, L. 1969, *Ap. J. (Letters)*, **156**, L63.
Baliunas, S. L., and Butler, S. E. 1980, *Ap. J. (Letters)*, **235**, L45.
Black, J. H., Dupree, A. K., Hartmann, L. W., and Raymond, J. C. 1980, *Ap. J.*, **239**, 502.
Blades, J. C. 1980, *M.N.R.A.S.*, **190**, 33.
Blades, J. C., and Meaburn, J., 1980, *M.N.R.A.S.*, **190**, 59p.
Blitz, L. 1979, *Ap. J. (Letters)*, **231**, L115.
Boggess, A., *et al.* 1978*a*, *Nature*, **275**, 372.
_____. 1978*b*, *Nature*, **275**, 377.
Bohlin, R. C., Savage, B. D., and Drake, J. F. 1978, *Ap. J.*, **224**, 132.
Bosma, A. 1978, *Proefschrift*, University of Groningen.
Bregman, J. N. 1980, *Ap. J.*, **236**, 577.
Bruhweiler, F. C., Kondo, Y., and McCluskey, G. E. 1980, *Ap. J.*, **237**, 19.
Burton, W. B. 1976, *Ann. Rev. Astr. Ap.*, **14**, 275.
Burstein, P., Borken, R. J., Kraushaar, W. L., and Sanders, W. T. 1977, *Ap. J.*, **213**, 405.
Chevalier, R. A., and Oegerle, W. R. 1979, *Ap. J.*, **227**, 398.
Cowie, L. L., Jenkins, E. B., Songaila, A., and York, D. G. 1979, *Ap. J.*, **232**, 467.
Cowie, L. L., and York, D. G. 1978, *Ap. J.*, **220**, 129.
de Boer, K. S., Koornneef, J., and Savage, B. D. 1980, *Ap. J.*, **236**, 769 (Paper II).
de Boer, K. S., and Lamers, H. J. G. L. M. 1978, *Astr. Ap.*, **69**, 327.
de Boer, K. S., and Morton, D. C. 1979, *Astr. Ap.*, **71**, 141.
de Boer, K. S., and Savage, B. D. 1980, *Ap. J.*, **238**, 86 (Paper III).
Faber, S. M., and, Gallagher, J. S. 1979, *Ann. Rev, Astr. Ap.*, **17**, 135.
Feast, M. W., Thackeray, A. D., and Wesselink, A. J. 1960, *M.N.R.A.S.*, **121**, 337.
Gondiadzki, D., and Jech, A. 1970, in *IAU Symposium 38, The Spiral Structure of Our Galaxy*, ed. W. Becker and G. Contopoulos (Dordrecht: Reidel), p. 157.
Gunn, J. E., Knapp, G. R., and Tremaine, S. D. 1979, *A. J.*, **84**, 1181.
Habing, H. J. 1969, *B.A.N.*, **20**, 177.
Hindman, J. V., and Kerr, F. J. 1970, *Australian J. Phys. Ap. Suppl.*, **18**.
Hulsbosch, A. N. M. 1975, *Astr. Ap.*, **40**, 1.
Jenkins, E. B., 1978*a*, *Ap. J.*, **219**, 845.
_____. 1978*b*, *Ap. J.*, **220**, 107.
Kepner, M. 1970, *Astr. Ap.*, **5**, 44.
Koornneef, J., and McGee, R. X. 1981, in preparation.
Kurucz, R. L., and Peytremann, E. P. 1975, *Smithsonian Ap. Obs. Spec. Rep., No.* 362.
Mathewson, D. S., Schwarz, M. P., and Murray, J. D. 1977, *Ap. J. (Letters)*, **217**, L5.
McKee, C. F., and Ostriker, J. P. 1977, *Ap. J.*, **218**, 148.
Morton, D. C. 1975, *Ap. J.*, **197**, 85.
_____. 1978, *Ap. J.*, **222**, 863.
Morton, D. C., and Smith, W. H. 1973, *Ap. J. Suppl.*, **26**, 333.
Nachman, P. M., and Hobbs, L. M. 1973, *Ap. J.*, **182**, 481.
Nousek, J. A., Fried, P. M., Sanders, W. T., and Kraushaar, W. L. 1980, in preparation.
Oort, J. H., and Plaut, L. 1975, *Astr. Ap.*, **41**, 71.
Osborne, J. L. 1975, in *Origin of Cosmic Rays*, ed. J. L. Osborne, and A. W. Wolfendale (Dordrecht: Reidel), p. 203.
Raymond, J. C., Cox, D. P., and Smith, B. W. 1976, *Ap. J.*, **204**, 290.
Ross, J. E., and Aller, L. H. 1976, *Science*, **191**, 1223.
Sanduleak, N. 1968, *A. J.*, **73**, 246.
_____. 1970, *CTIO Contr.* No. 89.
Sanders, W. T., Kraushaar, W. L., Nousek, J. A., and Fried, P. M. 1977, *Ap. J. (Letters)*, **217**, L87.
Savage, B. D., and Bohlin, R. C. 1979, *Ap. J.*, **229**, 136.
Savage, B. D., and de Boer, K. S. 1979, *Ap. J. (Letters)*, **230**, L77 (Paper I).
Savage, B. D., and Mathis, J. S. 1979, *Ann. Rev. Astr. Ap.*, **17**, 73.
Savage, B. D., and Jeske, N. A. 1981, *Ap. J.*, in press.
Schmidt, M. 1965, in *Galactic Structure*, ed. A. Blaauw and M. Schmidt (Chicago: University of Chicago Press), p. 513.
Shapiro, P. R., and Field, G. B. 1976, *Ap. J.*, **205**, 762.
Shapiro, P. R., and Moore, R. T. 1976, *Ap. J.*, **207**, 460.
Shull, J. M. and York, D. G. 1977, *Ap. J.*, **221**, 803.
Shull, J. M., York, D. G. and Hobbs, L. M. 1977, *Ap. J. (Letters)*, **211**, L139.
Spitzer, L. 1956, *Ap. J.*, **124**, 20.
Sturrock, P. A., and Stern, R. 1980, *Ap. J.*, **238**, 98.
Thuan, T. X. 1975, *Ap. J.*, **198**, 307.
Ulrich, M.-H., *et al.* 1980. *M.N.R.A.S.*, **192**, 561.
Verschuur, G. L. 1973*a*, *Astr. Ap.*, **27**, 73.
_____. 1973*b*, *Astr. Ap.*, **27**, 407.
Walborn, N. R. 1977, *Ap. J.*, **215**, 53.
_____. 1980, *Ap. J. (Letters)*, **235**, L101.
Wannier, P., Wrixon, G. T., and Wilson, R. W. 1972, *Astr. Ap.*, **18**, 224.
Weisheit, J. G. 1978, *Ap. J.*, **219**, 829.
Weisheit, J. G., and Collins, L. A. 1976, *Ap. J.*, **210**, 299.
York, D. G., and Kinahan, B. F. 1979, *Ap. J.*, **228**, 127.

Note added in proof.—Shull, Snow, and York (1981, *Ap. J.*, submitted) redetermined Si II *f*-values based on *Copernicus* and *IUE* spectra. Revisions for Table 2 are: λ1808.00, $f=0.0055$; and λ1526.71, $f=0.23$. This implies shifting the two leftmost Si points of Fig. 5; notably the entry near $\log Ab_{\odot} f\lambda = 9.7$ shifts to 10.2. The Si II column density limits given in this paper have to be revised downward by ~0.3 in the log.

K. S. DE BOER AND B. D. SAVAGE: Department of Astronomy, 475 N. Charter St., University of Wisconsin, Madison, WI 53706